JOURNAL OF MATERIALS SCIENCE 31 (1996) 3893–3913

Review
The interfacial properties of aramid/epoxy model composites

M. C. ANDREWS, D. J. BANNISTER, R. J. YOUNG
Manchester Materials Science Centre, UMIST/University of Manchester, Grosvenor Street, Manchester, M1 7HS, UK

Many attempts have been made to measure, evaluate and improve the level of interfacial adhesion in aramid/epoxy composites. Different surface treatments have been developed in order to promote chemical bonding between the fibre and the matrix but it is found that most of the surface treatments developed have shown little or no improvement in the level of interfacial adhesion. The interfacial properties of a model composite are often determined by measuring the interfacial shear strength using micromechanical test methods that employ different loading configurations. However, the values of interfacial shear strength determined using different test methods are found to be dependent upon the variation of localized stress in the samples due to the different loading configurations and often give different results. Using Raman spectroscopy it is shown that the strain-dependent shift of the 1610 cm^{-1} aramid Raman band can be used to determine the point-to-point variation of axial fibre strain along aramid fibres embedded in epoxy resin matrices from which the interfacial properties can be derived. The interfacial properties of aramid/epoxy model composites have been determined using Raman spectroscopy where the properties of the fibre, including different surface treatments, and the matrix have been changed systematically. The results are reviewed here and compared to those obtained using conventional micromechanical test methods. It is also demonstrated that the Raman technique can be used to characterize the interfacial properties of aramid/epoxy model composites deformed using different micromechanical test methods. In this way the interfacial properties can be determined at different loading levels enabling the progressive failure of the fibre/matrix interface to be monitored and defined accurately.

1. Introduction

1.1. Aramid fibre/epoxy resin adhesion

It is well known that the level of interfacial adhesion is of fundamental importance in determining the transfer of stress from a relatively low modulus matrix to a high modulus fibre in a discontinuous fibre-reinforced composite system. Low levels of interfacial shear strength have been reported for aramid/epoxy composites [1–6] indicating a need to improve the adhesive properties and interactions of the fibre/matrix interface. These findings have promoted the development of aramid fibre adhesion by means of chemical modifications [2, 3, 6], plasma surface treatments [4, 5] and the coating of aramid fibres with epoxy-based polymeric emulsions and solutions [7, 8].

The interfacial mechanisms that determine the adhesive properties of the interface have been reviewed by Allen [9] and with particular reference to aramid/epoxy composite systems by Kalantar and Drzal [10]. The promotion of aramid/epoxy adhesion has concentrated primarily upon the development of chemical covalent bonding between the resin matrix and the fibre surface. The applied surface treatments are designed to act in some respects as coupling agents in that chemical covalent bonds form between reactive groups on the fibre surface and the matrix. The principle of most chemical reactions [2, 3, 6] and plasma gas treatments [4, 5, 11] is to attach reactive amine groups to the fibre surface that could form covalent bonds between reactive sites in a neighbouring epoxy resin matrix. The exact nature of the bonding mechanism between plasma treated fibres and epoxy molecules is not clear since the plasma surface treatment can cause surface roughening and also induce additional reactive sites through the formation of free radicals [11] that may lead to ionic bonding. Any improved interfacial adhesion could therefore be a combination of chemical bonding, ionic bonding and mechanical interlocking. This is also true of the chemical modifications developed using bromination, ammonolysis and nitration reactions [2, 3]. The reactions required to attach the reactive amine groups to the fibre surface are known to cause surface roughening which is indicated by the undesirable reduction in the tensile properties of the fibres. Increased surface

0022–2461

roughening can facilitate fibre/matrix adhesion provided that favourable wetting is achieved. It has been demonstrated [12] that removing the antistatic sizing treatment increases the surface energy of the fibres which reduces the wettability of the fibres. The importance, however, of mechanical interlocking on the adhesive properties is expected to be small since strong adhesive bonds can be achieved by extremely smooth surfaces [9] where the degree of mechanical interlocking is small.

Shrinkage of the resin during cure from elevated temperatures around the fibre can cause thermal stresses due to the differences in the thermal expansion coefficients of the two components [1]. Thermal stresses induced during cure can increase the level of surface contact thus enhancing frictional interactions but also impose axial and radial strains on the fibre [1]. A similar effect can be achieved during deformation of the composite due to the Poisson's ratio difference between the fibre and the matrix. If the axial Poisson's ratio of the fibre is lower than that of the matrix then the matrix will contract radially upon the application of a tensile stress to a greater extent than the fibre. Compressive stresses at the interface can increase the interfacial surface contact and bonding. If the axial Poisson's ratio of the fibre is greater than that of the matrix then the fibre will contract radially more than the matrix which can facilitate interfacial debonding. The axial Poisson's ratio of aramid fibres is similar to that of the epoxy resin matrix (~ 0.35) [10] so the effect of a Poisson's ratio mismatch is expected to be small. This may be compared with carbon fibre/epoxy composites where the axial Poisson's ratio of carbon fibres is reported to be between 0.22–0.25 [10]. Therefore both thermal stresses and Poisson's ratio mismatch are expected to have an effect upon the interfacial properties of carbon/epoxy composites compared with those of aramid/epoxy composites [1] prepared under similar conditions.

1.2. Micromechanical test methods

A major problem in determining the interfacial properties and failure mechanisms of a composite system is the accuracy and repeatability of measuring the level of adhesion between the fibre and the matrix. The degree of interfacial adhesion may be characterized with respect to macromechanical properties such as interlaminar shear strength or transverse tensile strength or by employing micromechanical test methods. Several micromechanical test methods have been developed to determine the interfacial properties of model composites. The methods developed have been based upon the deformation of a single-fibre, partially or fully embedded in a resin matrix, until failure of the fibre, the matrix or the interface occurs. The most common methods, shown schematically in Fig. 1, include pull-out [13], microbond [14, 15], fragmentation [16] and microindentation [17] tests. The microindentation test is unsuitable for testing aramid/epoxy composites because the aramid fibres split and fibrillate when a load is applied to the end of the aramid fibre.

The level of interfacial adhesion is usually characterized by the interfacial shear strength parameter, τ_s. It is often calculated by making assumptions of stress distributions and material properties which may not give an accurate picture of the state of stress in the system. Although the tests appear to be rather simple and easy to perform, the complex state of stress due to the loading of the samples can often lead to variable, scattered results even for the same fibre/matrix system [18]. In order to measure the interfacial shear strength, τ_s, the samples are often continuously loaded until complete interfacial failure has occurred. It is generally accepted however, particularly with respect to the fibre pull-out test, that the maximum interfacial shear stress occurs at a lower loading level and represents the initiation of matrix yielding and/or interfacial failure [19, 20] which then propagates along the fibre/matrix interface.

Pull-out [4, 6, 7], microbond [14, 21] and fragmentation tests [1, 21, 22] have been employed frequently to evaluate the level of interfacial adhesion in an aramid/epoxy model composite system. The tests were generally used in order to observe the effect of different fibre surface treatments or the effect of matrix curing temperatures upon the level of interfacial adhesion or to compare the interfacial properties of different fibre/matrix systems. In some cases small differences in the values of interfacial shear strength have been observed for aramid fibres with different surface treatments [21, 22] but large differences have been reported using different test methods for similar aramid/epoxy system [1, 21, 22]. This can be seen in Table I which summarizes some of the values of interfacial shear strength of aramid/epoxy model composites calculated by several workers using conventional micromechanical test methods. Similar discrepancies have been reported for carbon fibre/epoxy resin systems [18].

Using micromechanical test methods it is often possible to observe differences in the values of maximum load required to cause complete interfacial failure for fibre/matrix systems where the properties of the fibre, the matrix, or the surface treatments applied to the fibres have been changed systematically. The assumption of constant interfacial shear stress along the interface generally applied in the analyses of micromechanical test methods is generally not appropriate for calculating accurate values of interfacial shear strength. So in order to understand fully the initiation and progressive interfacial failure mechanisms of the fibre/matrix interface it is important to monitor continuously the point-to-point variation of fibre stress and interfacial shear stress in the model composite at each loading level.

1.3. Raman spectroscopy

Using Raman spectroscopy apparatus such as that shown schematically in Fig. 2 it is possible to obtain well-defined Raman spectra for a number of different high-performance fibres. Fig. 3 shows a typical Raman spectrum obtained from a high-modulus aramid fibre. It is found that certain Raman bands

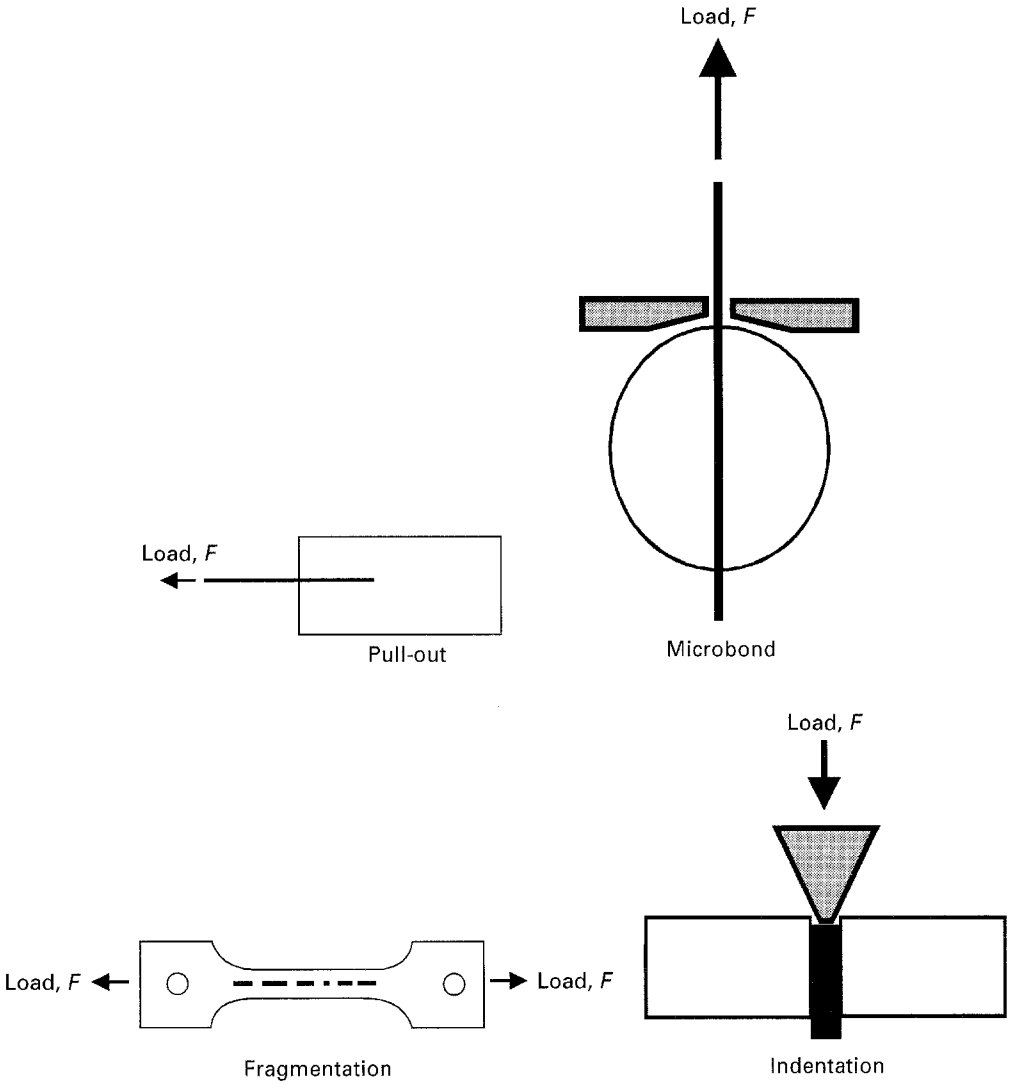

Figure 1 Micromechanical test methods.

shift upon the application of a stress to the fibre and that the strain dependent shift of the 1610 cm^{-1} aramid Raman band (Fig. 4) can be used to determine the distribution of strain along aramid fibres embedded in an epoxy resin matrix, shown schematically in Fig. 5, and described elsewhere [34–38].

It recent years the stress-dependent Raman band shifts associated with the deformation of high-performance fibres [23–31] have been used to follow the deformation of a fibre embedded in a resin matrix [32–40]. In the case of aramid and carbon fibres the shift of the Raman bands with stress or strain can be used to calibrate the strain at any point along the fibre embedded in the resin matrix. It is then possible to map the distribution of strain along a short, discontinuous fibre in a model composite and then derive the variation of interfacial shear stress along the interface. The Raman technique was first used to map the distribution of strain along a polydiacetylene single crystal fibre embedded in an epoxy resin matrix [32, 33]. The technique has subsequently been extended to monitor the stress and strain in aramid [34–38], carbon [39, 40] and polyethylene fibres [41–44] in an epoxy resin matrix and also ceramic fibres [45] in a glass matrix. By monitoring the stress along the fibre it is possible to study the effect of fibre [38, 42], matrix [46, 47] and interfacial properties [38] upon the level of adhesion in a model composite system. In addition to this, the effect of fibre surface treatments [36–40, 48] and processing conditions [47] can be assessed. With so many variables contributing to the transfer of stress in a composite system it is important to use samples where the fibre and matrix properties, including the fibre surface treatments are controlled systematically.

Raman and fluorescence spectroscopy have recently been used to study the distribution of stress and strain in micromechanical pull-out [20, 40–43, 49, 50], microbond [49, 51], fragmentation [37, 40, 48, 49, 52] and microindentation (fluorescence spectroscopy) [53] samples for a number of fibre/matrix systems. The application of Raman spectroscopy to the study of composite micromechanics has considerable advantages over conventional micromechanical test methods by monitoring accurately the variation of interfacial shear stress along the interface at different loading levels. This is in contrast to a single value of interfacial shear strength obtained using conventional test techniques which is usually calculated following complete failure of the fibre matrix interface. The distribution of fibre stress and fibre strain can also be determined along small fragments during a fragmentation test [37, 40, 48, 49, 52] by employing the same

TABLE I Values of interfacial shear strength, τ_s, for aramid fibre/epoxy resin model composites obtained using different micromechanical test methods

Fibre	Matrix	Curing schedule	Test method	Interfacial shear strength, τ_s (MPa)		
				Surface treatment		
				Sized	De-sized	Ref.
Kevlar 49	Ciba Geigy 6010 Resin + 956 Hardener	3 h 120 °C	Pull-out	–	34	4
	Ciba Geigy LY 5052 Resin + HY 5052 Hardener	7 days RT	Pull-out	10	–	20
	Der 331 Resin + DEH 26 Hardener	1–3 days 20 °C + 3 h 80 °C + 3 h 120 °C	Microbond	25	20	21
	Der 331 Resin + DEH 26 Hardener	1–3 days 20 °C + 3 h 80 °C + 3 h 120°C	Fragmentation	33	28	21
	Der 331 + Der 732 Resin + DEH 26 Hardener	3 h 80 °C	Fragmentation	32–35	–	22
	Der 331 Resin + DETA 26 Hardener	25 °C	Fragmentation	–	17	1

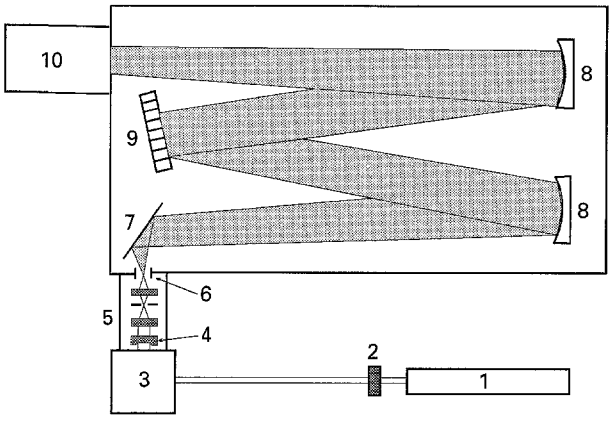

Figure 2 Schematic diagram of the Raman spectroscopy apparatus used for the collection of Raman spectra; (1) Laser, (2) Laser band-pass filter, (3) Optical microscope, (4) Holographic notch filter, (5) Spatial filter assembly, (6) Spectrometer slits, (7) Plane mirror, (8) Concave mirror, (9) Diffraction grating, (10) CCD camera.

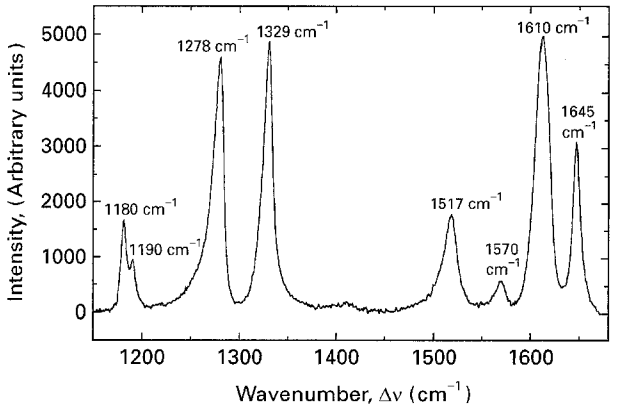

Figure 3 Raman spectrum of an aramid fibre between 1100 cm^{-1} to 1700 cm^{-1}.

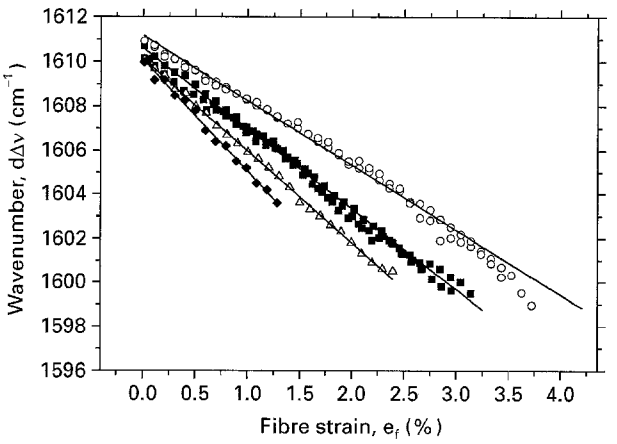

Figure 4 Dependence of the peak position of the 1610 cm^{-1} aramid Raman band upon fibre strain for four different aramid fibres, (○) Twaron LM, (■) Twaron HM, (△) Kevlar 49, (◆) Kevlar 149.

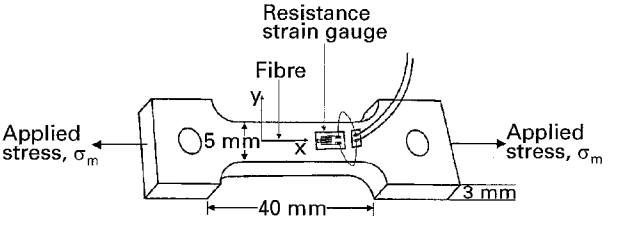

Figure 5 Schematic diagram of a single-fibre model composite.

technique used to determine the distribution of strain along short fibres fully-embedded in a resin matrix. By monitoring the distribution of fibre strain at different matrix strains it is possible to derive the interfacial shear stress prior to, during and following fibre fragmentation. In this way not only can the stress along

the fragment be measured but also the fragment length can be determined which is often difficult using conventional test techniques [1, 21, 22] due to the fibrillar fracture associated with aramid fibres.

The pull-out geometry is a more complex situation. The Raman band position of the asymmetric and symmetric C–C stretch has, however, been used to determine the stress along polyethylene fibres partially embedded in an epoxy resin matrix during a pull-out test [41–43]. The preparation of aramid fibre/epoxy resin samples is difficult since short embedded lengths ($L_e \leqslant 1000$ μm) are generally required. It has, however, recently been demonstrated [20, 49, 50] that it is possible to determine the state of stress or strain along aramid fibre pull-out samples in order to study the effect of fibre surface treatments and matrix curing characteristics even where the embedded length is only 100 μm. The variation of interfacial shear stress with distance along the fibre can be determined at each level of loading enabling the progressive failure of the interface to be monitored compared with the sudden catastrophic interfacial failure associated with conventional micromechanical test methods.

Raman spectroscopy is a powerful technique for studying the macroscopic deformation of a polymer through the deformation of the molecular structure [28]. Since it is an optical method there is usually little or no damage to the sample except through the direct application of stress. It has been shown however, that argon ion laser radiation, with a wavelength of 488 nm, can damage aramid fibres and result in a severe reduction in the tensile strength of the fibres [54]. The molecular deformation can be studied for a fibre both in air and in a resin matrix. Raman spectroscopy will therefore find increasing use in the analysis of fibre deformation in high-performance composites and can be used in situations where no analytical solutions exist or to confirm analytical solutions to particular theories of fibre reinforcement.

1.4. Stress transfer models

Many theoretical analyses have been developed to account for the transfer of stress in a discontinuous fibre-reinforced composite system. The tensile stresses are transferred to the fibre through a shearing mechanism at the interface which results in a distribution of stress along the length of the fibre. The first model to represent the transfer of stress in a composite was concerned with the deformation of the matrix and the fibre in the elastic state [55] and was developed using the well known shear-lag theory. The increased use of polymer matrices has led to the development of stress transfer models that account for plastic deformation and matrix yielding [16] and debonding [56–59]. Interfacial failure is often complicated by the fact that a reduction in stress transfer cannot be totally accounted for by one single mode of deformation. Partial-debonding models have, therefore, been developed [56–59] to represent the progressive failure of the fibre/matrix interface. If the stress along the fibre can be determined experimentally, at various loading levels, it is possible to determine the modes of stress transfer and interfacial failure by direct comparisons with the theoretical models.

1.5. Aim of the review

The aim of this paper is to review the interfacial properties of aramid/epoxy model composites and to ascertain the influence of the fibre and matrix properties and fibre surface treatments upon the adhesive properties of the fibre/matrix interface. The Raman technique can be used to determine the fibre strain and interfacial shear stress distribution profiles along short, aramid fibres embedded in single-fibre model composites where the properties of the matrix and the fibre surface treatments are changed systematically. It is demonstrated at low levels of matrix strain that for an aramid/epoxy model composite system the efficiency of stress transfer from the matrix to the fibre is dependent upon the elastic properties of the fibre and the matrix. In this case the distribution of fibre stress and interfacial shear stress can be quantified using shear-lag theory [55]. At high levels of matrix strain the interfacial properties are dominated by matrix yielding and debonding of the fibre/matrix interface.

The Raman technique can be extended to measure the interfacial properties of fragmented aramid fibres during a fragmentation test and also of an aramid fibre during pull-out from an epoxy resin block or resin droplet enabling the progressive failure of the fibre/matrix to be continuously monitored. For each test, the values of interfacial shear stress derived at each loading level may be compared with the single values of interfacial shear strength calculated using conventional analyses following complete failure of the fibre/matrix interface. The experimental data may also be compared to theoretical models that account for elastic behaviour, matrix yielding and partial-debonding of the fibre matrix interface in order to obtain a full explanation of the deformation modes responsible for interfacial failure. By comparing the Raman data obtained using different test geometries similar modes of deformation are observed to be responsible for interfacial failure. Also the maximum values of interfacial shear stress calculated for each test are in close agreement which is in contrast to the considerable variation of interfacial shear strength values often reported using conventional micromechanical test methods and analyses [18].

2. Single-fibre model composites

2.1. Strain mapping

Fig. 6 shows the peak position of the strain sensitive 1610 cm^{-1} aramid Raman band along a short Kevlar 49 fibre, 1.8 mm long, embedded in a room-temperature-cured epoxy resin matrix, containing 38 pbw of hardener, at 0, 0.8, 1.6 and 2.4% strain. Upon application of a tensile stress to the composite sample the peak position of the 1610 cm^{-1} Raman band shifts to a lower wavenumber indicating a transfer of a tensile stress to the fibre. The strain in the fibre can be calculated from the calibration of the peak position

of the 1610 cm^{-1} band with fibre strain, e_f, for the Kevlar 49 fibre deformed in air shown in Fig. 4. In the calibration experiment in Fig. 4 the fibres had been subjected to axial tensile deformation with the laser beam polarized parallel to the fibre axes. Hence the band shifts determined in the composite specimens relate only to axial strains in the fibres even though the fibres might be subjected to complex states of stress.

Conversion of the data in Fig. 6 using the strain calibration curves in Fig. 4 enables the distribution of axial fibre strain, e_f, to be determined along the fibre in the epoxy resin matrix at different strain levels. In order to understand fully the transfer of stress from the matrix to the fibre it is necessary to analyse in detail the fibre strain distribution data at different matrix strains at both the left- and right-hand end of the fibre as shown in Fig. 7(a and b). The solid lines are a fit of the experimental data to a logistic sigmoid function with a correlation coefficient greater than 98%. It can be seen that in the unstrained case ($e_m = 0\%$) there is virtually no strain in the fibre. This implies that any residual stresses imposed on the fibre during cure of the epoxy resin matrix at room temperature are very small. As the matrix strain, e_m, increases, the strain in the fibre increases from the fibre ends up to a plateau value along the middle of the fibre. It is shown that the strain in the central region of the fibre is approximately equal to the matrix strain, thus indicating an efficient transfer of stress from the low modulus matrix to the high modulus reinforcing fibre. At high matrix strains ($e_m > 1.2\%$) the fibre strain increases from the fibre end at a slower rate than at lower matrix strains. The stress transfer length, l_t, is found to increase indicating a reduction in the efficiency of stress transfer. This can be seen more clearly in Fig. 8(a and b) which show the derived variation of interfacial shear stress, τ, with distance, x, along the left- and right-hand end of the Kevlar 49 fibre. The interfacial shear stress, τ, is derived using a force balance equilibrium [16] given by

$$\tau = E_f \frac{r}{2}\left[\frac{de_f}{dx}\right] \quad (1)$$

where E_f is the fibre modulus, r is the fibre radius and (de_f/dx) is the first derivative of the strain function with respect to x. The equation assumes a uniform tensile stress across the fibre and that all the shear is in the matrix. At matrix strains up to 1.2% the magnitude of the interfacial shear stress is a maximum at the fibre ends ($x = 0\ \mu m$) decreasing to zero at a distance, x, along the fibre equal to l_t. At matrix strains greater than 1.2% there is a reduction in the transfer of stress close to the fibre ends and, as will be discussed later, is a result of matrix yielding followed by debonding of the fibre/matrix interface. The interfacial shear stress at the fibre ends is reduced and the maximum peak value of interfacial shear stress is now located at a distance, x, along the fibre where $0 < x < l_t$. This behaviour has been observed repeatedly [34–38] but the exact mechanism of interfacial failure is often difficult to define.

The interfacial shear stress profiles for both the left- and right-hand ends are qualitatively similar. The maximum values of interfacial shear stress, τ_{max}, shown in Fig. 9 are also similar indicating that any stress relaxation during the time taken to obtain Raman spectra from the left-hand end of the fibre to the right-hand end is insignificant. Only at high matrix strains is there a significant variation in the values of τ_{max} between the two fibre ends which may be due to

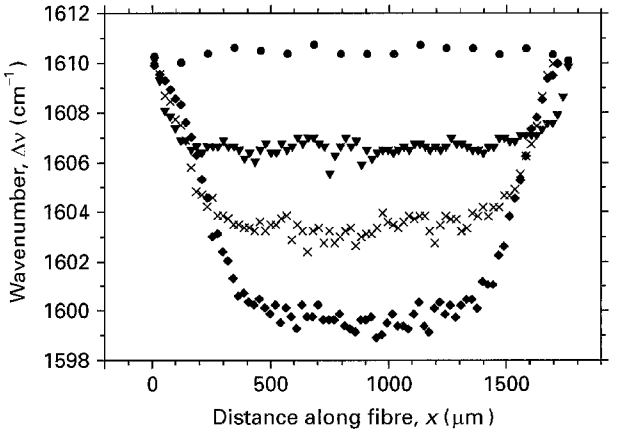

Figure 6 Variation of peak position of the 1610 cm^{-1} Raman band with distance along the length of a Kevlar 49 fibre in a model composite at levels of matrix strain, of (●) $e_m = 0\%$, (▼) $e_m = 0.8\%$, (×) $e_m = 1.6\%$ and (◆) $e_m = 2.4\%$.

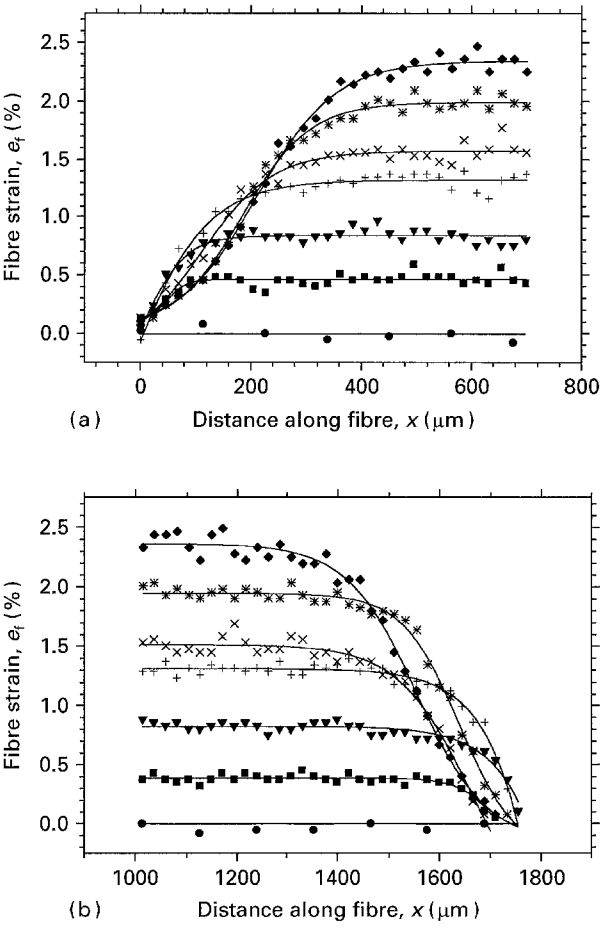

Figure 7 Variation of fibre strain with distance along (a) the left-hand end and (b) the right-hand end of a Kevlar 49 fibre in a model composite at levels of matrix strain, of (●) $e_m = 0\%$, (■) $e_m = 0.4\%$, (▼) $e_m = 0.8\%$, (+) $e_m = 1.2\%$, (×) $e_m = 1.6\%$, (*) $e_m = 2.0\%$, (◆) $e_m = 2.4\%$.

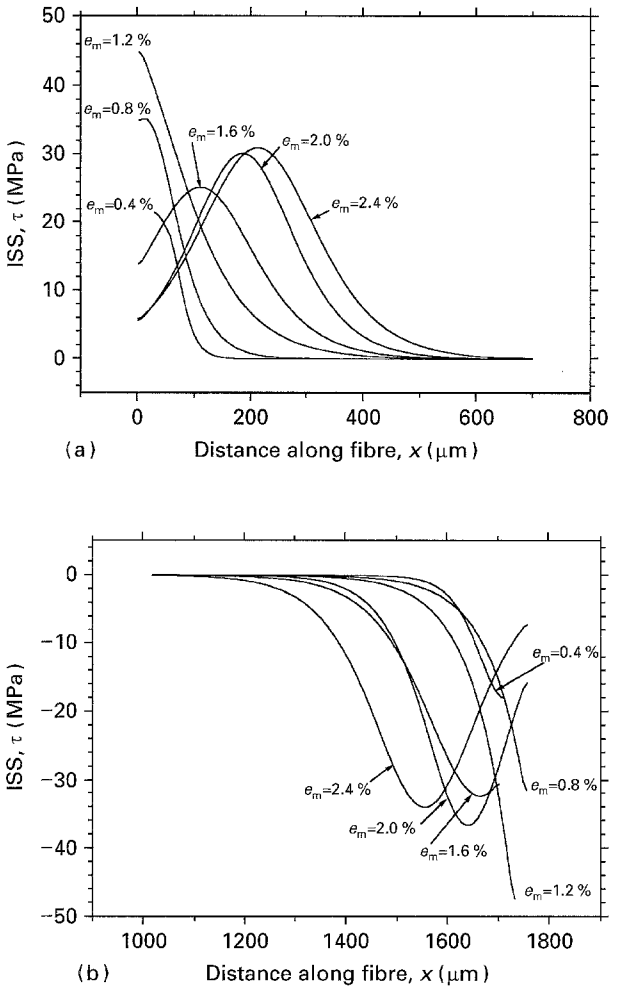

Figure 8 Derived variation of interfacial shear stress, τ, with distance along (a) the left-hand end and (b) the right-hand end of a Kevlar 49 fibre in a model composite at different levels of matrix strain.

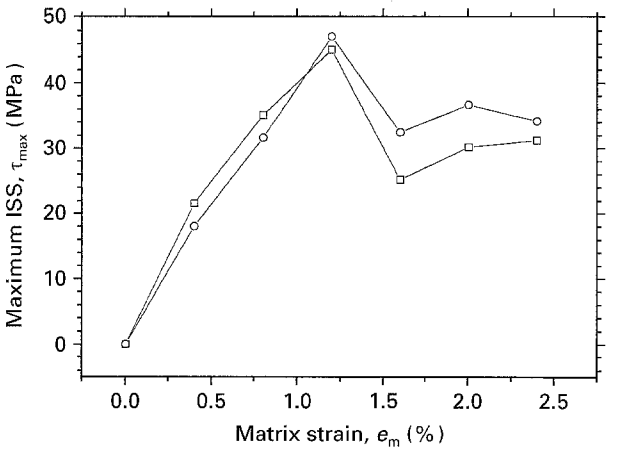

Figure 9 Dependence of maximum interfacial shear stress, τ_{max}, upon matrix strain for the left- (□) and right-hand (○) end of a Kevlar 49 fibre in a model composite.

different degrees of local interfacial failure close to the fibre ends.

2.2. Shear-lag analysis

The first theory to represent the stress distribution along a short reinforcing fibre in a low modulus matrix was presented by Cox in 1952 [55] using a shear-lag analysis. The theory assumes that;

(i) the fibre is isotropic,

(ii) both the fibre and the matrix remain in the elastic state during deformation,

(iii) there is a perfect bond between the fibre and the matrix at the interface,

(iv) there is no bonding across the fibre ends,

(v) the fibre can be represented by a uniform cylinder with a diameter equal to $2r$.

A model was proposed for a length of fibre, l, embedded in a matrix under a general strain, e_m. The transfer of load from the matrix to the fibre was determined by considering the displacement of a point, x, along the fibre to give the general expression [55]:

$$\frac{dF}{dx} = B(x_1 - x_2) \quad (2)$$

where F is the load on the fibre, x_1 is the displacement of the point, x, if the fibre is present, x_2 is the displacement of the same point, x, if the fibre is absent and B is a constant. A full derivation of the expression for the tensile fibre stress is given in Holister and Thomas [60]. Cox showed that for an applied matrix stress parallel to the fibre axis, the axial strain in the fibre can be given by [55]:

$$e_f = e_m\left[1 - \frac{\cosh\beta(l/2 - x)}{\cosh\beta\, l/2}\right] \quad (3)$$

for $0 < x < l$ where

$$\beta = \left[\frac{2G_m}{E_f r^2 \ln(R/r)}\right]^{\frac{1}{2}}$$

and E_f is the fibre modulus, e_m is the matrix strain, l is the fibre length, G_m is the shear modulus of the matrix, r is the fibre radius and R is the distance between neighbouring fibres. For a single fibre model composite, R may be represented by a cylinder of resin around the fibre into which the stress will decay radially [61]. The variation of interfacial shear stress along a fibre, determined by the Cox model can be derived by differentiating Equation 3 and substituting into Equation 1 to give:

$$\tau = E_f e_m\left[\frac{G_m}{2E_f \ln(R/r)}\right]^{\frac{1}{2}} \frac{\sinh\beta(l/2 - x)}{\cosh\beta\, l/2} \quad (4)$$

It is extremely useful to examine the applicability of such an analysis to the experimental data. Fig. 10 shows the fibre strain distribution along the left-hand end of a Kevlar 49 fibre embedded in a resin matrix at strain levels of 0.8 and 2.4% strain. The solid lines have been calculated from shear-lag analysis using Equation 3. It is clearly shown that while the data have an impressive fit to the shear-lag theory at low matrix strains ($e_m \leqslant 1.2\%$) considerable differences between the experimental data and the theoretical data are observed at high matrix strain levels ($e_m = 2.4\%$) particularly in the region close to the fibre

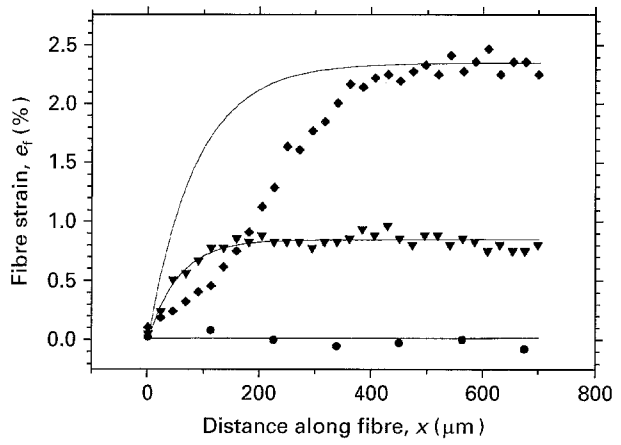

Figure 10 Variation of the fibre strain near the left-hand end of Kevlar 49 fibre in an epoxy resin matrix. The solid lines have been calculated from shear-lag theory using Equation 3. (●) $e_m = 0\%$, (▼) $e_m = 0.8\%$, (◆) $e_m = 2.4\%$.

end. This is not surprising since the theoretical shear-lag analysis does not account for either matrix yielding or interfacial failure that may occur in the highly-stressed region at the fibre end.

Another problem of the shear-lag model is in the determination of the parameter, R, for a single-fibre model composite. The value of R is often varied in order to obtain the best fit to the experimental data [34, 35, 38]. The effect of this parameter upon the fibre strain distribution is demonstrated in Fig. 11a which shows the experimental strain distribution data along a Kevlar 49 fibre at 0.4% and 0.8% strain. The solid lines have been calculated from shear-lag theory using different geometrical ratio values, R/r, of 5, 10 and 15. As R/r increases the strain distribution broadens. The best fit of the data was found to be when $R/r = 5$ i.e. $R = 30$ μm which is considerably less than half the width of the single-fibre composite sample used to obtain the experimental data.

It would appear that a better fit of the experimental data to the shear-lag theory would be obtained if the shear-lag theory accounted for a finite strain at the fibre end. For a discontinuous fibre deformed in a resin matrix, the experimental fibre strain data obtained using the Raman technique [35, 62] tend to indicate that the strain at the fibre end is not equal to zero and is usually of the order of 0.1–0.2%. This may be due to either bonding across the fibre end, not accounted for in the shear-lag analysis, or the geometry of the cut fibre end. Fan and Hsu [62] demonstrated for polydiacetylene fibres, with square-cut and tapered ends, embedded in an epoxy resin matrix than the fibre strain at the fibre end was highly dependent upon the geometry of the cut fibre. The aramid fibres employed in this study were cut with ceramic scissors. This avoided fibrillar fracture at the fibre end to a large extent but tended to deform the fibre end thus forming a 'mushroom' shaped geometry as shown elsewhere [34]. The fibre strain distribution at the aramid fibre end in Fig. 11a is similar to the fibre strain distribution obtained for a square-cut polydiacetylene fibre embedded in an epoxy resin matrix [62].

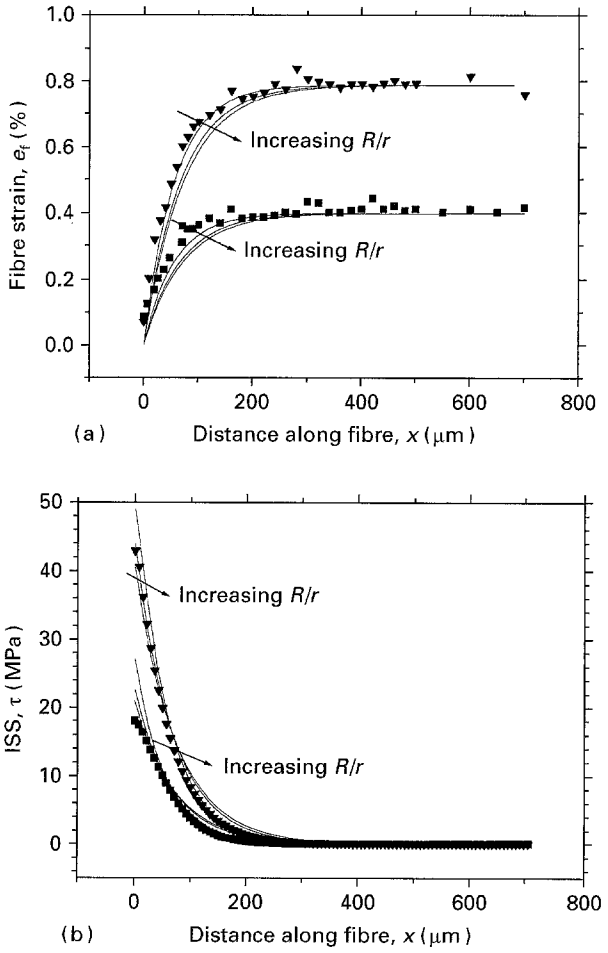

Figure 11 Variation of (a) fibre strain and (b) interfacial shear stress with distance along a Kevlar 49 fibre in a resin matrix at (■) $e_m = 0.4\%$ and (▼) $e_m = 0.8\%$ matrix strain. The solid lines have been calculated from shear-lag theory where $R/r = 5$, 10, and 15.

It is evident that the geometry of the cut fibre end and the geometrical ratio, R/r, have a significant effect upon the predicted interfacial properties of the model composite. This is demonstrated in Fig. 11b which shows the derived variation of interfacial shear stress from the strain distribution data in Fig. 11a using a force balance equilibrium. The experimental data have a close fit with the derived interfacial shear stress data calculated from shear-lag theory using Equation 4. The maximum values of interfacial shear stress at the fibre end decreases as the geometrical aspect ratio, R/r, increases.

The experimental interfacial shear stress values near to the fibre end at 0.8% matrix strain have a close fit to the theoretical data whereas the interfacial shear stress values at 0.4% matrix strain are slightly lower than those predicted by shear-lag theory. This may be due to either the geometry of the cut fibre end or to the experimental curve fitted to the strain distribution data from which the interfacial shear stress was derived. It is clearly shown that the experimental fibre strain (Fig. 11a) and interfacial shear stress data (Fig. 11b) at low matrix strains ($e_m \leqslant 1.2\%$) have impressive fits with the shear-lag model proposed by Cox. This demonstrates that the transfer of stress from the matrix to the fibre is determined by the elastic

properties of the fibre and the matrix and that, in these circumstances, there is a good adhesive bond at the interface.

2.3. Matrix yielding

It has been shown so far that the behaviour of stress transfer in an aramid/epoxy model composite at low matrix strains can be modelled using conventional shear-lag theory where the mechanical properties of the resin matrix and the aramid fibre are considered to be essentially linear elastic [34–38]. The power of the Raman technique is readily demonstrated at higher strain levels where plastic deformation and interfacial debonding can occur. It was shown in Fig. 9 that the maximum value of interfacial shear stress, τ_{max}, was $\sim$43 MPa which is close to the shear yield stress of the resin matrix [46,47] calculated using a pressure-dependent yield criterion [63].

In order to study the effect of the matrix properties upon stress transfer in an aramid/epoxy model composite, the fibre strain and interfacial shear stress distributions have been determined along Kevlar 49 fibres embedded in room-temperature-cured epoxy resin matrices containing different levels (20, 25, 30 and 38 pbw) of hardener and hence with different mechanical properties [46,47]. Fig. 12a shows the variation of fibre strain with distance, x, along the left-hand end of a Kevlar 49 fibre embedded in an epoxy resin matrix containing only 20 pbw of hardener. No residual stresses were observed in the unstrained case. As the matrix strain is increased the distribution of fibre strain is similar to that predicted by shear-lag theory. It is shown clearly, however, that the fibre strain increases at a much slower rate for the composite containing only 20 pbw compared with the data shown in Fig. 7a for the similar model composite containing 38 pbw hardener.

The derived values of interfacial shear stress, shown in Fig. 12b are also considerably lower than the data shown in Fig. 7b. It is interesting however, to note that for each sample containing different amounts of hardener that the transfer of stress at the fibre ends is reduced at matrix strains in excess of 1.2%. This is clearly shown in Fig. 13 where the values of maximum interfacial shear stress, τ_{max}, are plotted for each level of matrix strain for a series of aramid/epoxy systems made with different levels of hardener. It can be seen that τ_{max} initially increases with matrix strain reaching a maximum value where $0.8\% \leqslant e_m \leqslant 1.2\%$. At matrix strain levels greater than 1.2%, τ_{max} decreases with matrix strain. It is clear from Fig. 13 that the maximum interfacial shear stress is dependent upon the structure and mechanical properties of the epoxy resin matrix. This can be seen more clearly by comparing the interfacial shear stress data in Fig. 13 with the compressive stress/strain data in Fig. 14 where the curves are the same shape. The maximum interfacial shear stress, τ_{max}, increases due to an increase in the shear yield stress of the resin as the level of curing agent is increased.

Fig. 15 shows the variation of maximum interfacial shear stress, for a matrix strain of 1.0% with the shear

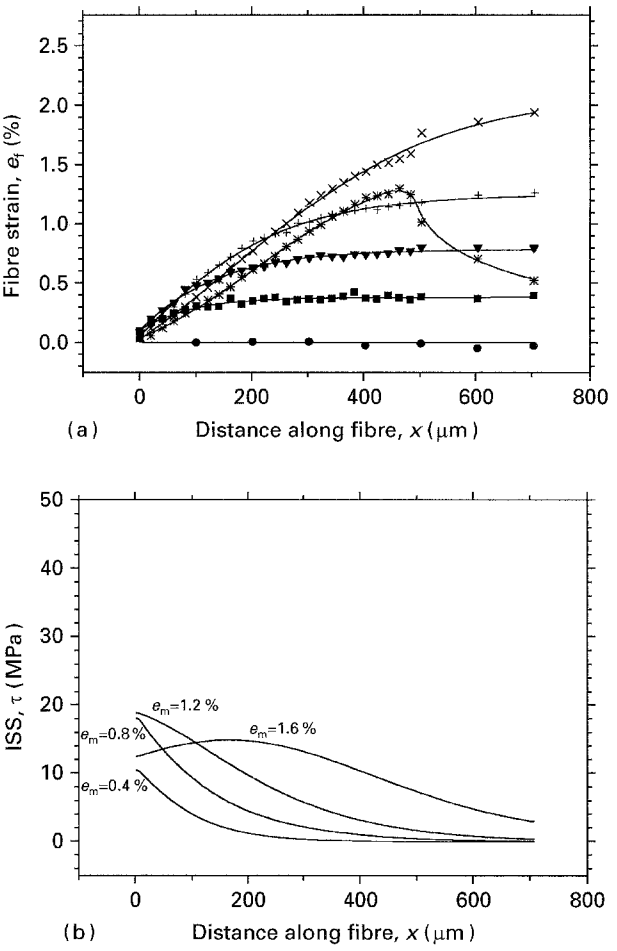

Figure 12 Variation of (a) fibre strain and (b) interfacial shear stress with distance along the left-hand end of a Kevlar 49 fibre in an epoxy resin matrix containing 20 pbw hardener at levels of matrix strain of; (●) $e_m = 0\%$, (■) $e_m = 0.4\%$, (▼) $e_m = 0.8\%$, (+) $e_m = 1.2\%$, (×) $e_m = 1.6\%$ and (∗) $e_m = 2.0\%$.

yield stress, τ_y, of the resin matrix, calculated using a pressure dependent yield criterion [63], for each of the four, room-temperature cured resin formulations employed. It is found that the values of maximum interfacial shear stress correlate well with the values of shear yield stress of the epoxy resin matrix. The similar trend in the two measurements implies very strongly that shear yielding of the epoxy resin matrix takes place at the fibre ends when the elastic shear-lag behaviour beaks down. The transfer of stress is consistent with the behaviour predicted by Kelly and Tyson [16] for a plastically deformed model composite where there is a good interfacial adhesion.

2.4. Thermal stresses

The effect of epoxy resin curing conditions upon stress transfer in a model composite has also been investigated [1,47]. Fig. 16a shows the variation of fibre strain along the left-hand end of a Kevlar 49 fibre in the epoxy resin matrix, containing 38 pbw of hardener, post-cured at 80 °C. In the unstrained case, $e_m = 0\%$, the fibre has been compressed to -0.25%. This compressive strain induced in the post-cured specimens is due to fibre extension in the axial direction, due to its negative thermal expansion coefficient [1], combined

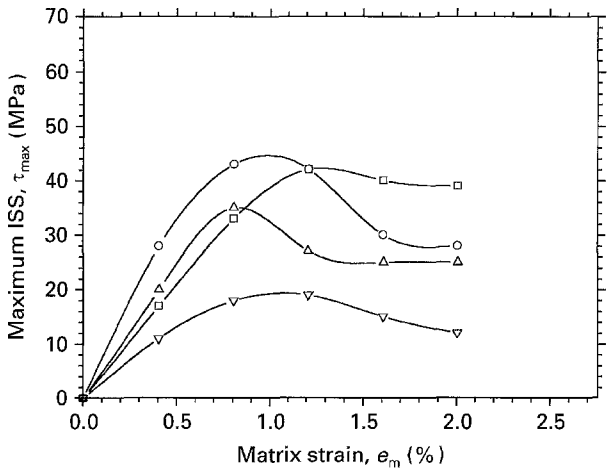

Figure 13 Dependence of maximum interfacial shear stress, τ_{max}, upon matrix strain for Kevlar 49 fibres in room temperature cured epoxy resin matrices containing levels of hardener of; (□) 38 pbw, (○) 30 pbw, (△) 25 pbw and (▽) 20 pbw.

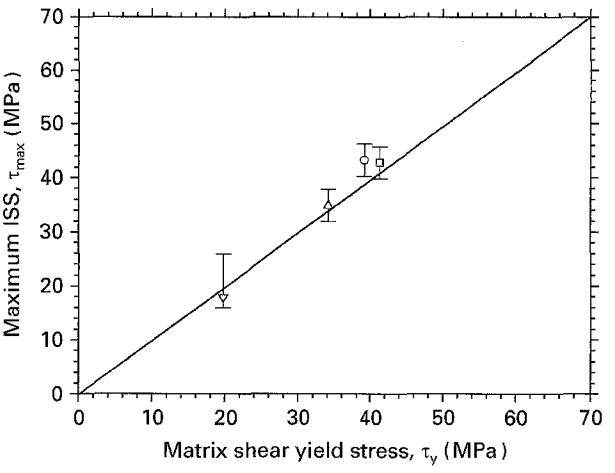

Figure 15 Dependence of τ_{max} upon shear yield stress of the epoxy resin matrices containing different levels of hardener at 1% strain. The levels of the hardener are; (□) 38 bpw, (○) 30 bpw, (△) 25 pbw and (▽) 20 pbw.

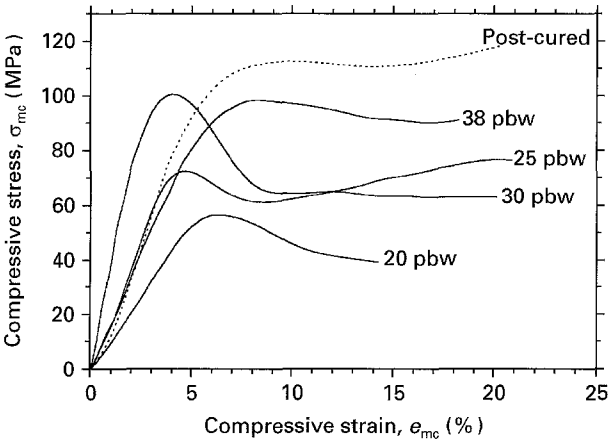

Figure 14 Compressive stress–strain curves for the different epoxy resin formulations.

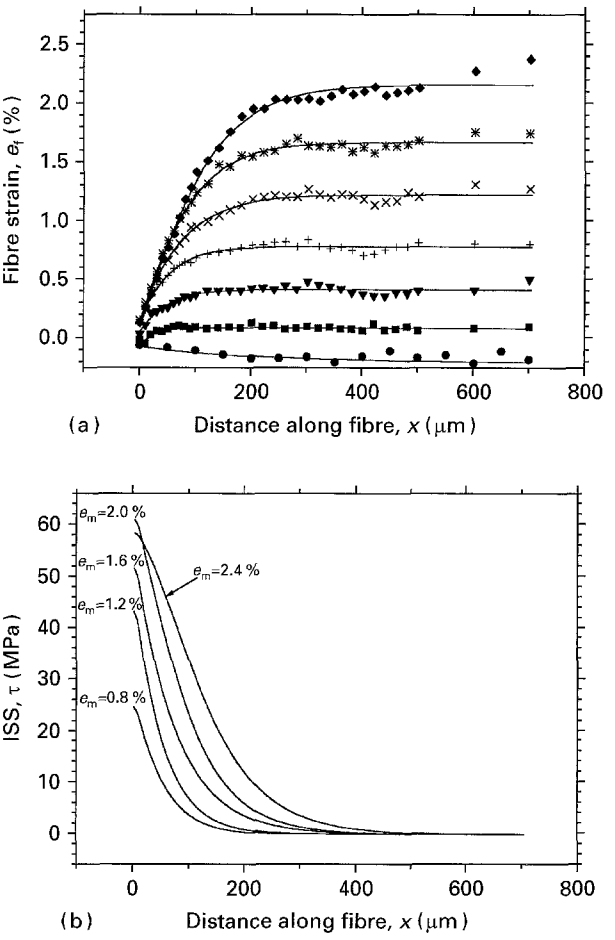

Figure 16 Variation of (a) fibre strain and (b) interfacial shear stress with distance along a Kevlar 49 fibre in an epoxy resin matrix post-cured at 80 °C. The data were taken at e_m vlaues of; (●) 0%, (■) 0.4%, (▼) 0.8%, (+) 1.2%, (×) 1.6%, (*) 2.0% and (◆) 2.4%.

with shrinkage of the resin matrix [1] around the fibre caused by cooling from the elevated temperature. The value of thermal residual strain, e_{res}, developed along the aramid fibres during cure can be derived from the definition of the coefficient of thermal expansion [64]

$$e_{res} = \int_{T_0}^{T_c} \alpha_f - \alpha_m \, dT \qquad (5)$$

where α_f and α_m are the axial coefficients of thermal expansion of the fibre and the matrix respectively, T_c is the curing temperature (80 °C) and T_0 is room temperature (23 °C). Using the literature values of $\alpha_f = -5.72 \times 10^{-6}\,°C^{-1}$ and $\alpha_m = 70 \times 10^{-6}\,°C^{-1}$ [1] a value of $e_{res} = -0.43\%$ is obtained for the residual strain in the fibre calculated using Equation 5. This theoretical value of residual fibre strain is higher than the experimental value of -0.25% shown in Fig. 16a. The reason for the difference between the two values will depend upon the values of α_f and α_m, whether the glass transition temperature, T_g, is less than the curing temperature, T_c, and also the fact that kink band formation can relieve the compressive strain in the fibre [65, 66].

As the matrix strain is increased, the fibre strain increases from the fibre end up to a maximum plateau value along the middle of the fibre in a similar manner to that shown in Fig. 7a for a Kevlar 49 fibre room-temperature cured model composite. It must be noted,

however, that the maximum strain in the fibre is less than the matrix strain at all strain levels up to 2.4%. It is shown that the distribution of strain along the fibre is similar to that predicted by shear-lag theory even when $e_m = 2.0\%$ indicating very little evidence of matrix yielding at the fibre/matrix interface. This is confirmed by the distribution of interfacial shear stress along the fibre, shown in Fig. 16b, where the interfacial shear stress is a maximum at the fibre end and decreases to zero at a distance, x, along the fibre for all matrix strain levels between 0.8% and 2.4%.

The maximum values of interfacial shear stress at the fibre end for the post-cured epoxy resin sample are higher than the maximum values of interfacial shear stress for the room-temperature cured resin samples, as shown in Fig. 7b, at each level of maximum fibre strain. This increase in interfacial shear stress cannot be totally accounted for by the increase in the tensile and compressive yield stress of the resin since the maximum interfacial shear stress is much higher than the shear yield stress of the post-cured resin, which is ~ 45 MPa [47]. Radial stresses at the fibre/matrix interface are expected to be small in an aramid/epoxy composite because the fibre and matrix will shrink radially by a similar amount since the radial thermal expansion coefficient of the fibre and matrix are similar [1]. However, if the fibre is axially compressed, as shown in Fig. 16a when $e_m = 0\%$, then the fibre will expand radially due to its Poisson's ratio and hence compressive radial stresses at the fibre/matrix interface will be generated. In this case the radial stresses might be relieved by the applied tensile stress. It is apparent that there must be some thermal clamping since no evidence of interfacial failure can be observed from the fibre strain and interfacial shear stress distributions in Fig. 16(a and b) close to the end of the Kevlar 49 fibre in the post-cured resin matrix. This is in contrast to the room-temperature cured sample shown in Fig. 7(a and b) where interfacial failure was observed close to the fibre end at high matrix strains indicated by a reduction in the maximum values of interfacial shear stress shown in Fig. 9 where $e_m \geqslant 1.6\%$.

The results obtained using the Raman technique are in contrast to the findings of Kalantar and Drzal [1] that showed no increase in the values of interfacial shear strength with increasing cure temperature. The values of interfacial shear strength were, however, calculated using fragmentation tests and analyses. The technique employed here has enabled the interfacial properties of the model composite to be determined at different matrix strains without having to deform the samples to high strains in order to induce fibre fracture.

2.5. Fibre surface treatments

The effect of fibre surface treatments upon the level of interfacial adhesion in a model composite is usually characterized using conventional micromechanical test methods [1, 4, 6, 7, 14, 21]. The Raman technique has, however, recently been employed in order to study the effect of surface treatments applied to aramid fibres upon the transfer of stress in a model composite [34–38, 67]. Most commercial grades of aramid fibre are generally coated with a surface finish or size [8] in order to improve handling and more importantly to improve the level of adhesion with a resin matrix. The distribution of fibre strain has been determined along untreated [67] and commercially surface-treated [34–37] Kevlar 49 fibres in single-fibre model composites. The distribution of fibre strain has also been determined along de-sized Kevlar 49 fibres [36, 37] where attempts have been made to remove the tenacious adhesion-promoting size [21, 36, 37, 68]. Only at high matrix strains were noticeable differences observed between the distributions of fibre strain and interfacial shear stress for the sized and de-sized and untreated fibres.

The Raman technique has also been used to compare the distributions of fibre strain along aramid fibres with different surface treatments [38] where the chemistry of the fibre surface treatment has been controlled systematically [7, 8]. This is demonstrated in Fig. 17(a and b) which shows the variation of fibre strain with distance, x, along an untreated Twaron HM fibre and a surface-activated Twaron HMA fibre in the epoxy resin matrix. The adhesion activation consists of a proprietary treatment with an epoxy-containing finish [8]. At low strain levels, $e_m \leqslant 1.2\%$, the fibre-strain distributions are qualitatively similar. The behaviour is consistent with that predicted by shear-lag theory [55]. The effect of fibre surface treatment becomes more apparent at high matrix strains, $e_m > 1.2\%$. The surface activated Twaron HMA fibres have good interfacial adhesion indicated by the shear-lag type behaviour at each level of matrix strain up to 2.0%. At high matrix strains the level of adhesion between the untreated Twaron HM fibre and the matrix is reduced close to the fibre end due to debonding of the fibre/matrix interface [38].

Fig. 18(a and b) shows the derived interfacial shear stress along the fibres in Fig. 17(a and b). At low matrix strains the behaviour is similar to that predicted by shear-lag theory [55]. In the case of the untreated Twaron HM fibre the interfacial shear stress at high matrix strains is reduced close to the fibre end. The maximum value of interfacial shear stress moves away from the fibre end indicating progressive interfacial failure along the fibre. In the case of the surface-activated Twaron HMA fibre the maximum value of interfacial shear stress increases at the fibre end with increasing matrix strain up to ~ 45 MPa which is close to the shear yield stress of the epoxy resin matrix [46]. At matrix strains $> 1.0\%$ the interfacial shear stress is reduced close to the fibre end but not to the same extent as that observed for the untreated Twaron HM aramid fibres.

The effect of the fibre surface treatment upon the level of interfacial adhesion is summarized in Fig. 19 which shows the variation of the maximum interfacial shear stress, τ_{max}, with matrix strain, e_m. It can be seen that the values of maximum interfacial shear stress at low matrix strains are similar for both the untreated Twaron HM fibres and the surface activated Twaron HMA fibres. At high matrix strains the values of

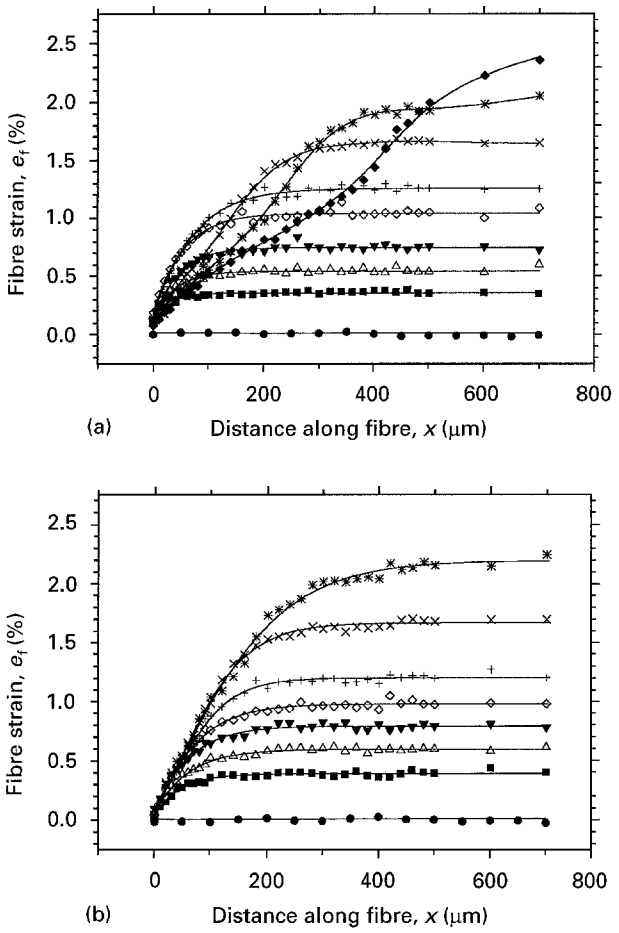

Figure 17 Variation of fibre strain with distance along the left-hand end of (a) an untreated Twaron HM fibre and (b) a surface-activated Twaron HMA fibre in single-fibre model composites at different strains. (e_m) levels of; (●) 0%, (■) 0.4%, (△) 0.6%, (▼) 0.8%, (◇) 1.0%, (+) 1.2%, (×) 1.6%, (∗) 2.0% and (◆) 2.4%.

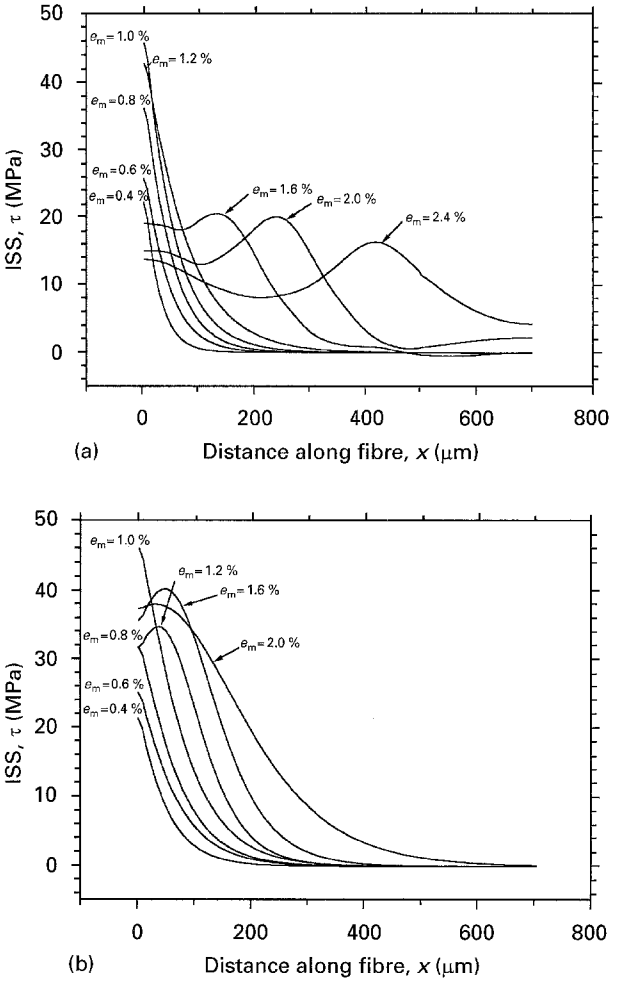

Figure 18 Derived variation of interfacial shear stress distance along the left-hand end of (a) and untreated Twaron HM fibre and (b) a surface-activated Twaron HMA fibre in single-fibre model composites at different levels of strain.

maximum interfacial shear stress are higher for the surface activated Twaron HMA fibres than those of the untreated Twaron HM fibres. It can also be seen that the maximum interfacial shear stress values at high strains for the surface activated fibres are close to the shear yield stress of the resin which is approximately 43 MPa [46]. This would indicate good interfacial adhesion along the fibre. For the untreated Twaron HM fibre the interfacial shear stress values at high strains are less than the shear yield stress of the resin. It will be shown next that this is a result of interfacial debonding near the fibre end.

2.6. Partially-elastic model

It has been demonstrated that the shear lag theory proposed by Cox [55] provides a suitable model for describing the strain distribution in an aramid/epoxy model composite at low levels of matrix strain where both the fibre and the matrix behave elastically. At higher levels of applied strain, i.e. when $e_m > 1.2\%$, it has been shown that the level of interfacial adhesion between the untreated fibres and the epoxy resin matrix is reduced. This leads to a breakdown of the Cox model which does not account for matrix yielding and interfacial debonding at the fibre end. In these

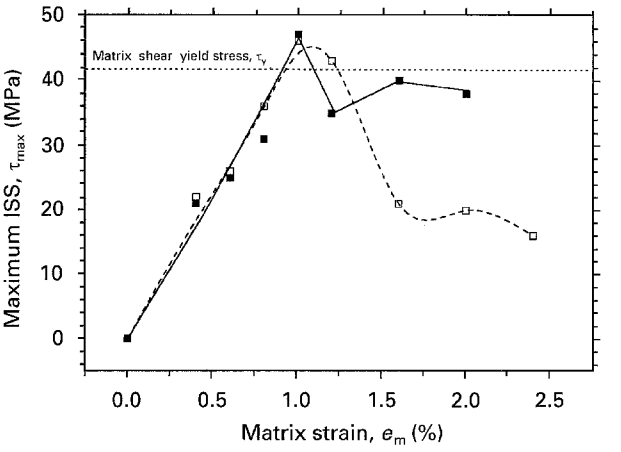

Figure 19 Dependence of maximum interfacial shear stress, τ_{max}, upon matrix strain for the, (□) Twaron HM and (■) Twaron HMA surface-activated fibres.

cases it is necessary to use other models to describe the inelastic behaviour.

In order to define the interfacial failure mechanisms in the untreated fibre/epoxy model composites it is useful to consider the partially-elastic model due to Piggott [56, 57]. If there is good adhesion between the fibre and the matrix the interfacial shear stress will be

a constant along the interface and will be equal to the shear yield stress of the matrix [16, 56]. If there is poor interfacial adhesion between the fibre and the matrix, as in the case of some fibre reinforced polymers, the high shear stresses at the fibre ends can produce slippage of the fibre within the matrix [56]. The frictional interfacial shear stress in this region, τ_i, will be less than the shear yield stress of the resin and will be a product of the coefficient of friction, μ, and the normal compressive stresses at the fibre/matrix interface. The normal stresses at the interface are due to residual stresses, σ_{res}, caused by differential contraction of the fibre and the matrix during manufacture, plus the Poisson's contraction of the matrix, $\sigma_{Poisson}$ when a stress is applied to the model composite [56]. It therefore follows that

$$\tau_i = -\mu[\sigma_{res} + \sigma_{Poisson}] \quad (6)$$

The value of σ_{res} is expected to be small since the model composite samples used in this study were all cured at room temperature. It has been shown, however, that aramid fibres in epoxy resin model composites post-cured at elevated temperatures [47] are subjected to residual compressive stresses, as shown in Fig. 16a.

The partially-elastic model assumes that there is perfect adhesion in the central region of the fibre. At the fibre ends debonding occurs over a distance $ml/2$ where m defines the point of transition from poor to good adhesion where $0 < m < 1$. The strain in the debonded region can be calculated by a force balance equilibrium to give [56, 57]

$$e_f = \frac{2\tau_i}{E_f r}\left(\frac{l}{2} - x\right) \quad (7)$$

where l is the fibre length, E_f is the fibre modulus and τ_i, is the frictional shear stress. There is a zone of perfect adhesion along the middle of the fibre of length $(1 - m)l$. The fibre strain distribution in the central region of the fibre will be defined by elastic behaviour where [56, 57]

$$e_f = e_m - \left[e_m - 2\tau_i sm/E_f\right]\frac{\cosh(nx/r)}{\cosh(ns(1-m))} \quad (8)$$

with

$$n^2 = \frac{E_m}{E_f(1+\nu_m)\ln(R/r)}$$

where e_m is the matrix strain, s is the aspect ratio l/d, ν_m is the Poisson's ratio of the matrix and all the other parameters are as defined earlier.

Fig. 20a shows the variation of fibre strain along the untreated Twaron HM fibre, shown in Fig. 17a, at high levels of matrix strain. The solid lines have been calculated from Equations 7 and 8 using the partially-elastic model [56, 57]. It is shown that the data are in good agreement with the partially-elastic model. At each level of strain there is an approximately linear increase in fibre strain from the fibre end along the fibre up to a distance equal to $x = ml/2$. This is the debonded region defined by the partially-elastic model due to the poor interfacial adhesion at high strain

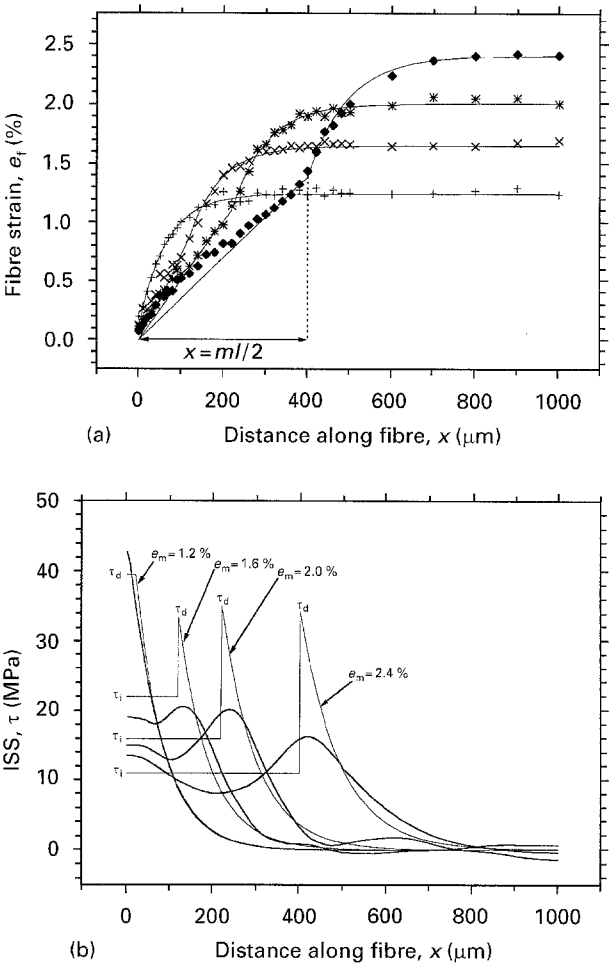

Figure 20 Variation of (a) fibre strain and (b) interfacial shear stress along the left-hand end of an untreated Twaron HM fibre in a model composite at levels of the matrix strain of; (+) $e_m = 1.2\%$, (×) $e_m = 1.6\%$ (*) $e_m = 2.0\%$ and (◆) $e_m = 2.4\%$. The solid lines have been calculated from the partially-elastic model using Equations 7, 8, and 9.

levels. As the matrix strain increases the debonded length $ml/2$ also increases along the interface. If shorter fibre lengths were used then interfacial failure would occur completely along the interface and the strain distribution would be approximately triangular [67]. It is shown that the theory does not fit the experimental data particularly well over the first 100 μm from the fibre end. This was also noted at low strain levels where the experimental data were fitted to the simple shear lag model. Similar factors must be applicable with respect to the geometry of the cut fibre end and also the possibility of bonding across the fibre end. The experimental data in this region appear to be in agreement with the theoretical model developed by Nairn *et al.* [59] to analyse the transfer of stress from the matrix to the fibre through an imperfect interface. This model uses Bessel–Fourier series stress functions to produce a three-dimensional axisymmetric analysis of the fragmentation test. Although the model was developed to represent the distribution of stress along a fibre fragment separated from a continuous filament these theoretical predictions have been found to be in agreement with the distribution of stress, derived from Raman data, along a short carbon fibre embedded in a resin matrix [59]. It should be noted however,

that the relatively simple partially-elastic model of Piggott [56, 57] has also been employed to represent adequately the transfer of stress along partially-debonded, fragmented carbon fibres [69].

The strain distribution in the central region of the fibre is dominated by elastic behaviour of both the fibre and the matrix. The best fit of the data was obtained using a value of 15 for the ratio R/r. Although this value cannot be measured directly, it is in close agreement with the values used at low strains where the data was fitted to the shear lag theory. The decrease in the shear modulus of the resin matrix with increasing strain has been accounted for at each level of applied strain.

According to the partially-elastic theory, the interfacial shear stress, τ_i in the debonded region, $0 \leqslant x \leqslant ml/2$, will be constant. The distribution of shear stress along the central region of the fibre controlled by elastic behaviour is given by [56, 57]

$$\tau = \frac{n}{2}\left[E_f e_m - 2\tau_i sm\right]\frac{\sinh(nx/r)}{\cosh(ns(1-m))} \quad (9)$$

Fig. 20b shows the derived experimental interfacial shear stress values shown in Fig. 18a along with the theoretical values calculated from Equation 9. The experimentally derived interfacial shear stress data vary more smoothly than the theoretical curves although they are qualitatively similar. The experimental interfacial shear stress data close to the fibre end are generally slightly higher than those predicted by the partially-elastic model in the debonded zone. The data appear to exhibit shear-lag behaviour over the first 100 μm from the fibre end as was indicated in the strain distribution data. This could be a result of the geometry of the cut fibre end restricting the level of debonding at the fibre end.

It is interesting to note that the initial value of the debonding shear stress, τ_d, at a matrix strain of 1.2% is close to the shear yield stress of the resin. The peak values of τ_d then decrease with increasing matrix strain and move away from the fibre end indicating a reduction in the level of interfacial adhesion propagating along the fibre. The maximum values of interfacial shear stress, τ_d, indicate the transition points along the fibre, equal to $ml/2$, which define a sharp transition from the debonded to the elastic region. The experimental data tend to indicate a transition region along the fibre from the debonded fibre end to the elastic central region as opposed to a singularity in τ. The values of τ_i are found to decrease with matrix strain. This is in contrast to the values of τ_i given by Equation 6 which predicts that the frictional shear stress should increase with matrix strain as $\sigma_{Poisson}$ increases. The reduction in the frictional shear stress at high strains may be due to the progressive breakdown of the interface.

3. Micromechanical test methods

3.1. Pull-out tests

The pull-out test and microbond test are frequently used in order to evaluate the interfacial shear strength of a fibre/matrix system [4, 6, 7, 14, 21]. The sample geometry and test procedure are relatively simple, however, there is usually a large variation between the values of interfacial shear strength calculated for each test [4, 18]. This arises due to the characteristic 'cloud' of measurements, as shown in Fig. 21 for aramid fibre/epoxy resin matrix pull-out samples with different embedded lengths. The interfacial shear strength, τ_s, is calculated conventionally from the relationship between the maximum load, F_{max}, required to extract a fibre from a resin matrix and is given by

$$\tau_s = \frac{F_{max}}{2\pi r L_e} \quad (10)$$

where r is the fibre radius and L_e is the embedded fibre length. This analysis assumes a yielding interface [16] where the interfacial shear stress is constant along the length of the fibre/matrix interface. Best-fit lines have been drawn through the data points in Fig. 21. Using Equation 10 the interfacial shear strength, τ_s, is calculated to be $\sim$10 MPa.

Chua and Piggott [70] have analysed the state of stress in the fibre where the fibre and the matrix both behave elastically. In this case the stress is transferred to the fibre without slip or yield and the tensile strain in the fibre, e_f, at any point along the embedded length is given by [70]

$$e_f = e_{app}\frac{\sinh[n(L_e - x)/r]}{\sinh ns} \quad (11)$$

where e_{app} is the strain applied to the fibre outside the resin, s is the fibre aspect ratio, L_e/r, ν_m is the Poisson's ratio of the matrix and all other terms are as defined previously.

The Raman technique has recently been employed to analyse the strain in an aramid fibre during pull-out from an epoxy resin block [20, 50]. It is shown that the progressive failure of the fibre/matrix interface can be monitored during a pull-out test [20] and that the behaviour can be modelled using a partially-elastic model [20, 56]. This is demonstrated in Fig. 22a which shows the distributions of fibre strain along a Kevlar 49 fibre pull-out sample with an embedded length,

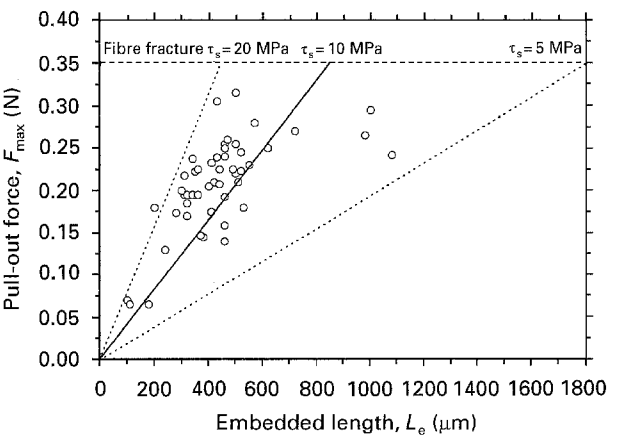

Figure 21 Experimental data showing the dependence of the pull-out force, F_{max}, upon embedded length, L_e, for Kevlar 49/epoxy resin pull-out samples.

$L_e = 1080\ \mu m$, for nominal applied strains ranging from 0.6–1.6%. This single Raman experiment provides a detailed insight into the three main stages of pull-out; elastic deformation, partial debonding and frictional pull-out.

At low strain levels, $e_{app} \leqslant 0.6\%$, the fibre strain decreases from a maximum value where the fibre enters the resin to approximately zero at the fibre end. The dashed line in Fig. 22a has been calculated using Equation 11 and indicates that this behaviour is quantitatively similar to the distribution of fibre strain predicted by shear-lag theory [70].

As the fibre strain outside the resin is increased the shear-lag theory becomes inadequate to model the corresponding fibre strain distributions. It is apparent from Fig. 22a, that debonding of the fibre/matrix interface has occurred and that the distribution of fibre strain is now defined by two distinct zones. The debonding model proposed by Piggott [56] assumes a constant frictional interfacial shear stress in the debonded region where the fibre strain is given by

$$e_f = \frac{2\tau_i}{rE_f}(L_e - x) \tag{12}$$

In the partially-debonded model of Piggott [56] the assumption that the strain distribution in the debonded region is defined by the embedded length appears to be invalid. From the strain distribution profiles shown in Fig. 22a it is clear that the linear decrease in strain in the debonded region can be extrapolated to a point $x = z$, where $z > L_e$. Equation 12 can be modified to give

$$e_f = \frac{2\tau_i}{rE_f}(z - x) \tag{13}$$

The fibre strain data in the bonded region are determined by elastic behaviour where the distribution of fibre strain is given by [50]

$$e_f = \frac{2\tau_i}{rE_f}[z - (1 - m)L_e]\frac{\sinh[n(mL_e - x)/r]}{\sinh nms} \tag{14}$$

The form of this equation is similar to the model that was applied to the distribution of fibre strain along untreated aramid fibres, fully-embedded in the same epoxy resin matrix, shown in Fig. 20a where m also defines the transition point from the debonded to the bonded region. The theoretical strain distributions can be generated from Equations 13 and 14 using suitable values for m and z. An excellent correlation is observed between the experimental data and the theoretical strain distributions, indicated by the solid lines in Fig. 22a, for all the partially-debonded data. It is shown that as the strain is increased there is stable propagation of the debond along the fibre/matrix interface.

Once the fibre has been completely debonded from the matrix the pull-out process is controlled by interfacial friction and the strain profile along the fibre is simply given by Equation 12. This is shown by the dotted line in Fig. 22a. In this case the fibre has pulled out partly from the resin block such that the embedded length is now only $\sim 650\ \mu m$.

Fig. 22b shows the interfacial shear stress distributions along the Kevlar 49 fibre in Fig. 22a. They have been derived using Equation 1 from the theoretical curves fitted to the strain profiles in Fig. 22a. In the totally bonded case the interfacial shear stress is a maximum where the fibre enters the resin and decreases along the fibre. The maximum value of interfacial shear stress is found to increase with applied strain until the strain reaches 0.6% after which point debonding is initiated. In the debonded region the interfacial shear stress is only ~ 5 MPa and is determined by friction. In the bonded region the interfacial shear stress increases from the embedded fibre end and reaches a maximum value of between 37–42 MPa at the point of transition, m, from the bonded to the debonded region. It is interesting to note that the interface has a maximum shear strength, τ_s, of the order of 42 MPa which is close to the shear yield stress of the epoxy resin matrix [46] and is also in agreement with the maximum value of interfacial shear stress observed for the fully-embedded fibre composites (Fig. 9).

The information obtained from the Raman data can be used to explain the features of typical force–displacement curves obtained for different fibre/matrix

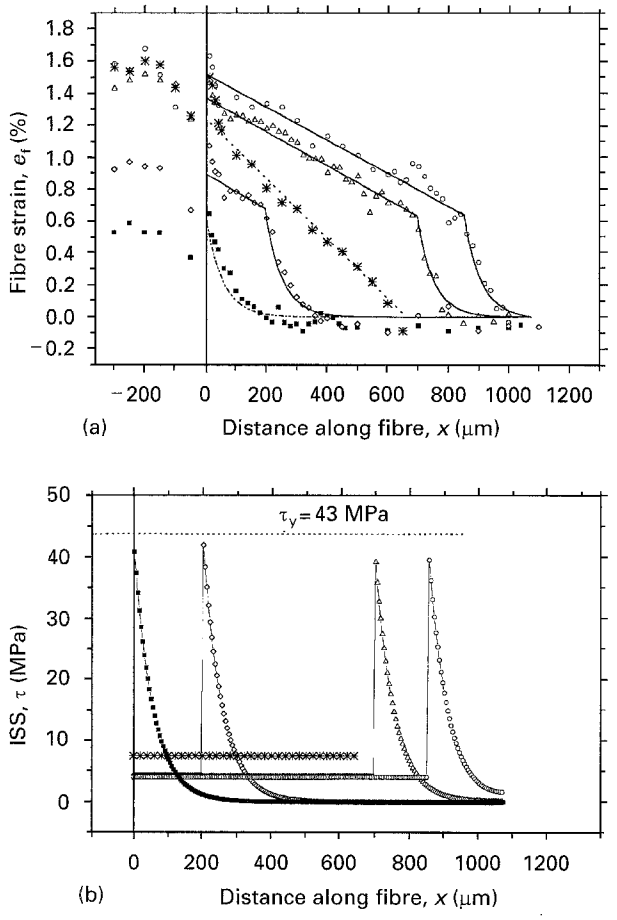

Figure 22 Variation of (a) fibre strain and (b) interfacial shear stress with distance along a Kevlar 49 fibre during a pull-out test at different levels of strain. The solid lines in (a) have been calculated from the partially-elastic model using Equations 13 and 14. At a normal strain ε_0 the elastic response is (■) 0.6% the partial debonding is (◇) 0.89%, (△) 1.37%, (○) 1.52% and the frictional pull out (∗) 1.24%.

systems [20]. The interfacial shear stress data can also be used to account for the different values of interfacial shear strength and the typical 'cloud' of scattered data, shown in Fig. 21, obtained using conventional pull-out test methods [21]. It has been demonstrated that for an aramid/epoxy pull-out sample [20] that the maximum interfacial shear strength, $\tau_s = \tau_d = \sim 43$ MPa and is dependent upon the shear yield stress of the resin [34–38]. Following debonding of the fibre/matrix interface the interfacial shear stress is determined by friction and is of the order of 5 MPa. It is shown in Fig. 21 that the interfacial shear strength calculated from the pull-out data is ~ 10 MPa and that all the data points lie between $5 \leqslant \tau \leqslant 20$ MPa. The frictional interfacial shear stress determined from other pull-out samples, analysed using Raman spectroscopy, has also been in the range 5–20 MPa [20]. It is therefore implied that all the samples have a similar value of interfacial shear strength, $\tau_s = 43$ MPa, but have different values of frictional interfacial shear stress, τ_i. This would seem to be reasonable since the strength of the interface may not vary significantly from specimen to specimen but the frictional shear stress, τ_i, is likely to be sensitive to factors such as local fibre diameter, the presence of kink bands and the geometry of the embedded fibre ends.

The Raman technique has enabled the progressive failure of the interface to be monitored and unlike conventional micromechanical test methods the values of maximum interfacial shear stress measured for the same fibre/matrix system using different test geometries are in agreement.

3.2. Microbond test

The microbond test may be considered as a geometrical variation of the pull-out test where the fibre is pulled out from a restrained resin droplet compared with the usual resin cylinder or rectangular block. Sample preparation may be difficult since in the case of aramid fibre/epoxy resin samples small droplets are generally required where the diameter of the droplet is less than 500 μm. The microbond technique has been used to determine the interfacial shear strength of an aramid/epoxy interface [21] where the surface chemistry of the aramid fibres had been changed. The assumption that the interfacial shear stress is constant along the entire length of the fibre/matrix interface has, however, been found to be inappropriate [49, 51, 71].

It has recently been demonstrated that the Raman technique can also be applied to study the deformation of an aramid fibre inside an epoxy resin droplet during a microbond test [49, 51, 71]. Fig. 23a shows the distributions of fibre strain along Kevlar 49 fibres inside two epoxy resin microbond droplets, determined from the point-to-point variation of the shift of the 1610 cm^{-1} aramid Raman band for an applied strain of 0.8%. The data correspond to two gripping geometries, one where the knife edges are close to the fibre and the other with the knife edges well separated. It can be seen that the fibre strain decays into the droplet and that the strain falls more rapidly when the knife edges are close together. The dashed curve indicates the fibre strain distributions for a conventional pull-out sample predicted by the Cox-type shear-lag model of Chua and Piggott [70] given by Equation 11. It can be seen that Equation 11 predicts the correct form of the behaviour however, the experimental fibre strain data decay more rapidly than predicted theoretically when the knife edges are close together and more slowly when they are separated. This behaviour is consistent with the results presented by Herrera–Franco and Drzal [15] where the stress in the microdroplet, determined using photoelastic methods and finite element analysis, was found to be dependent upon the position of the knife edges.

Fig. 23b shows the derived variation of interfacial shear stress along the Kevlar 49 fibres in the microbond samples shown in Fig. 23a. It can be seen that for both gripping geometries the shear stress decays into the droplet and is similar to the behaviour predicted by shear-lag theory. It is found however, that the decay is much more rapid when the grips are close together and that the maximum value of interfacial shear stress is of the order of 75 ± 15 MPa compared with 18 ± 3 MPa when the grips are far apart. The large difference between the values of interfacial shear stress confirms the fact that there is a complex stress field in the droplet that is highly dependent upon the

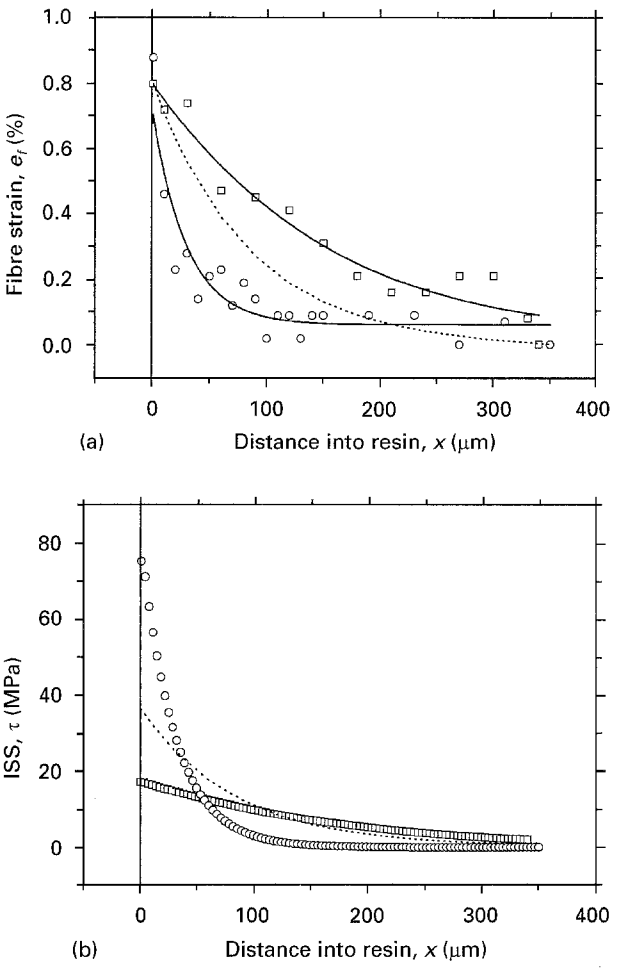

Figure 23 Variation of (a) fibre strain and (b) interfacial shear stress with distance along Kevlar 49 fibres in epoxy resin droplets during a microbond test. Two different loading configurations are shown, namely; (○) knife edges close and (□) knife edges apart. The dotted line is a theoretical fit.

position of the knife edge supports [15, 49, 71]. The complex stress field close to where the fibre enters the resin droplet may also produce shear within the fibre. In this case Equation 1, used here to derive the values of interfacial shear stress, is invalid.

Conventional analysis of the microbond test, using Equation 10, assumes that the interfacial shear stress is constant. Fig. 23b shows that this assumption is not correct although in the case where the knife edges are far apart it may be a fair approximation. Unfortunately however, the normal protocol of the microbond test [15] suggests that the separation of the grips should be as small as possible. The fact that the stress distribution in the droplet is extremely sensitive to the position of the knife-edge supports may also explain why the microbond test generally produces such scattered results [18].

3.3. Fibre fragmentation

Due to the high tensile failure strain of most aramid fibres (> 3%) and the fibrillar fracture associated with aramid fibres it is often difficult to analyse the interfacial properties of aramid fibre model composites using the fragmentation test. The presence of fibre fractures along a single fibre embedded in a resin matrix are usually monitored either optically using polarized light [1, 21, 22] or indirectly by the use of acoustic emission [22]. The disadvantage of these test methods is that they do not provide any direct information with respect to the stress in each fragment. The final fragment length is often referred to as the critical fragment length, l_c, and is usually calculated following saturation of the fragmentation process where the fragments are so short that the shear stresses along their lengths can no longer build up enough tensile stresses to cause any further fracture. The interfacial shear strength is often calculated using the simple equation [16]

$$\tau_s = \frac{r\sigma_f^*}{l_c} \quad (15)$$

where σ_f^* is the tensile strength of the fibre at the critical fragment length, l_c^*. Equation 15 simplifies the analysis of the fragmentation test in that the state of stress in each fragment is assumed to be uniform. This can lead to values of interfacial shear strength being under estimated.

It has recently been demonstrated that the Raman technique can be applied to the fragmentation process of carbon fibres in a resin matrix [40]. It is shown using the Raman technique that both the fragment length and the maximum stress in each fragment can be clearly defined. Raman spectroscopy has also been used to monitor the fragmentation process of high-modulus Kevlar 149 aramid fibres [52] where the strain to failure of the fibres is less than 1.5%. The importance of monitoring the interfacial properties at different loading levels can be clearly demonstrated.

At low matrix strains, $e_m \leqslant 1.2\%$, the distributions of fibre strain and interfacial shear stress are similar to those predicted by shear-lag theory [55] as shown in Fig. 24(a and b). The interfacial shear stress reaches

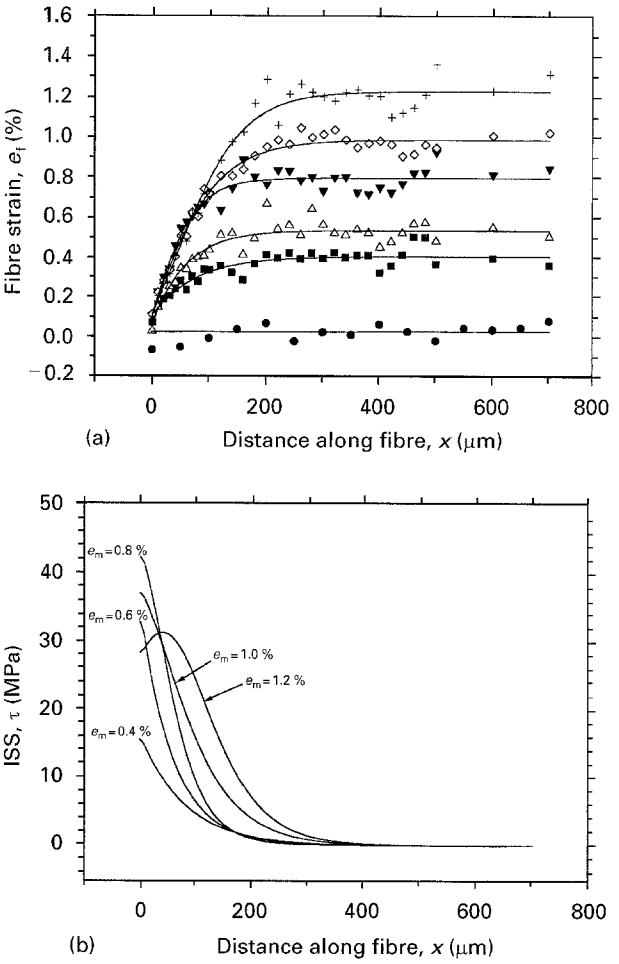

Figure 24 Variation of (a) fibre strain and (b) interfacial shear stress with distance along the left-hand end of a Kevlar 149 fibre in an epoxy resin matrix at levels of the matrix strain of; (●) $e_m = 0\%$, (■) $e_m = 0.4\%$, (△) $e_m = 0.6\%$, (▼) $e_m = 0.8\%$, (◇) $e_m = 1.0\%$ and (+) $e_m = 1.2\%$.

a maximum value of ~42 MPa where $e_m = 0.8\%$ and is again close to the shear yield stress of the resin matrix. This behaviour has been observed repeatedly [20, 36–38, 46] for several aramid fibre/epoxy model composite systems and indicates that the maximum value of interfacial shear stress is highly dependent upon the mechanical properties of the resin matrix. When the matrix strain is increased to 1.5% the failure strain of the aramid fibre is exceeded and the fibre breaks into two fragments (Fig. 25a). Increasing the matrix strain to 2.0% results in one of the fragments breaking into two smaller fragments (Fig. 25b). It is evident that the maximum strain in each fragment, e_f^{max} is lower than the strain in the matrix for $e_m = 2.0\%$ and it therefore follows that the fragmented fibre offers very little reinforcement.

The solid lines in Fig. 25(a and b) have been fitted using a cubic spline function [72]. This enables the variation of interfacial shear stress with distance, x, along the fibre to be derived accurately using Equation 1. This is demonstrated in Fig. 26(a and b) for the fibre strain distributions shown in Fig. 25(a and b). When fibre fragmentation occurs, the interfacial shear stress profiles become more complex than at low strains (Fig. 26(a and b)) with maximum values of interfacial shear stress, τ_{max}, located close to both the fibre ends and to the points of fracture along the fibre.

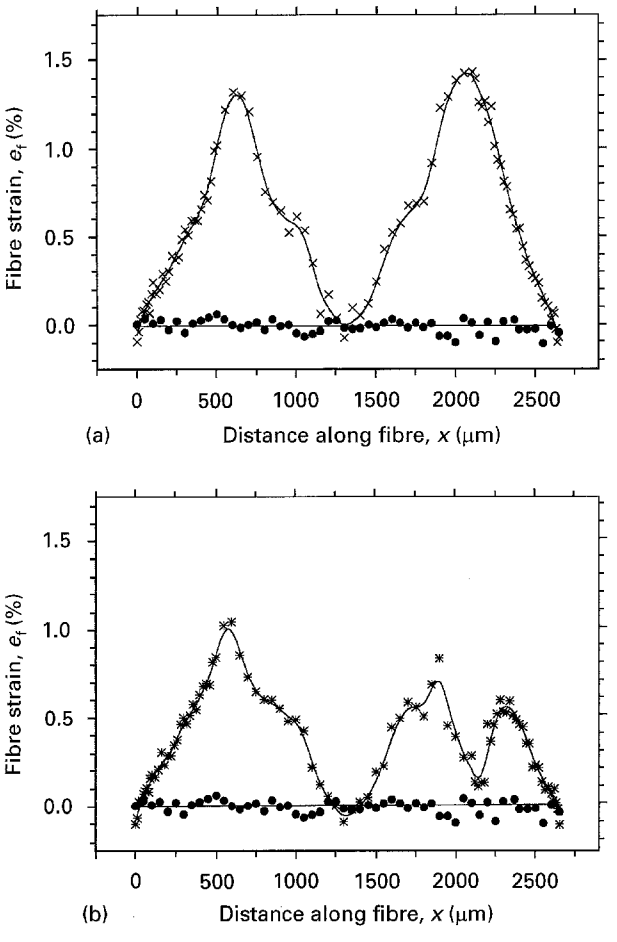

Figure 25 Variation of fibre strain along a fragmented Kevlar 149 fibre embedded in an epoxy resin matrix at; (×) a, 1.5% (*) b, 2.0% and (●) 0% strain.

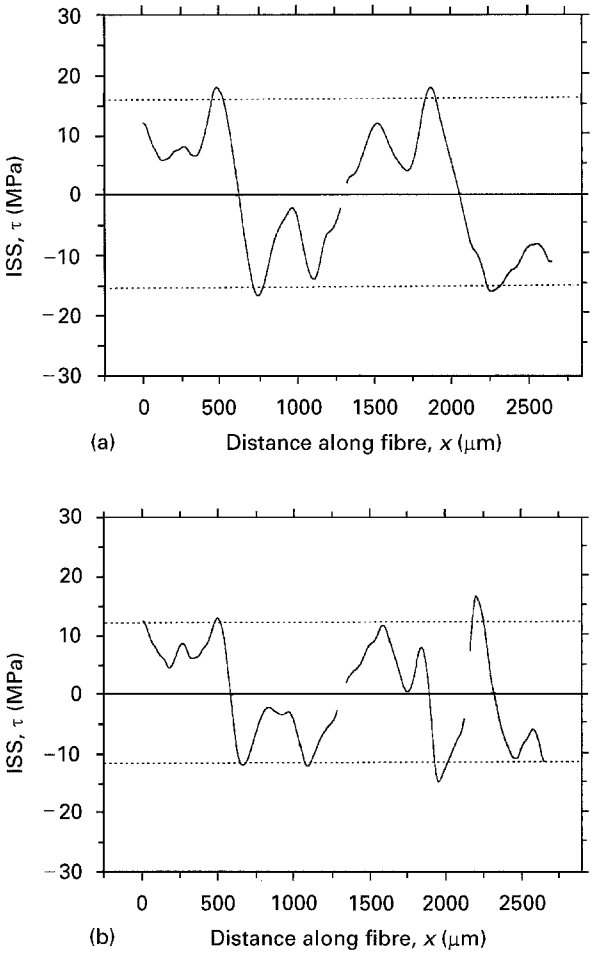

Figure 26 Derived variation of interfacial shear stress along a fragmented Kevlar 149 fibre embedded in an epoxy resin matrix at (a) 1.5% and (b) 2.0% strain.

The dotted lines in Fig. 26(a and b) indicate the average values of maximum interfacial shear stress at the fibre and fragment ends.

Conventional fragmentation procedures using either acoustic emission or polarized light techniques rely upon the precise determination of the critical fragment length, l_c, and the tensile strength of the fibre, σ_f^*, at the critical fragment length, in order to calculate the interfacial shear strength, τ_s. If the maximum stress, σ_f^{max}, in each fragment, of length, l_f, can be determined then the interfacial shear strength can be calculated by modifying Equation 15 to give

$$\tau_s = \frac{r\sigma_f^{max}}{l_f} \quad (16)$$

From the fragmented fibre strain distribution data, not only can the fragment length, l_f, be measured but also the maximum strain in each fragment, e_f^{max}, is known from which σ_f^{max} can be calculated. A value of 8.6 MPa has been calculated using Equation 16 from the fibre strain distribution data in Fig. 25(a and b).

Equations 15 and 16 both assume that the interfacial shear stress along the interface is constant. It is shown in Fig. 25(a and b) that while the distribution of fibre strain along each fragment is approximately triangular the interfacial shear stress data in Fig. 26(a and b) is by no means constant. If the interfacial shear stress is assumed to be constant along each fragment then the distribution of fibre strain should be approximately triangular. This is demonstrated in Fig. 27a where linear regression curves have been fitted to the strain distribution data in Fig. 25b. The variation of interfacial shear stress derived from the straight lines in Fig. 27a is shown in Fig. 27b. The uniform values of interfacial shear stress are approximately equal to ± 9 MPa and are lower than the maximum values of interfacial shear stress in Fig. 26b derived from the cubic spline curves fitted with greater accuracy to the same fibre strain distribution data.

The mean values of maximum interfacial shear stress, τ_{max}, indicated in Fig. 26(a and b), and interfacial shear strength, τ_s, derived from the fragmentation data appear to be considerably lower than the values of maximum interfacial shear stress, τ_{max}, shown in Fig. 24b, calculated at low strain levels, $e_m \leqslant 1.2\%$ for the Kevlar 149 model epoxy composite. This is clearly shown in Fig. 28 that gives the values of τ_{max} from Fig. 24b for the Kevlar 149 model composite along with the data calculated from fragmentation analysis. The circled data at 1.5 and 2.0% matrix strain shown in Fig. 28 indicate the mean values of maximum interfacial shear stress close to the fragment ends derived from fibre strain distribution profiles as indicated by the dotted lines in Fig. 26(a and b). The dotted line in Fig. 28 indicates the mean interfacial shear strength values calculated from Equation 16 using the conventional fragmentation analysis.

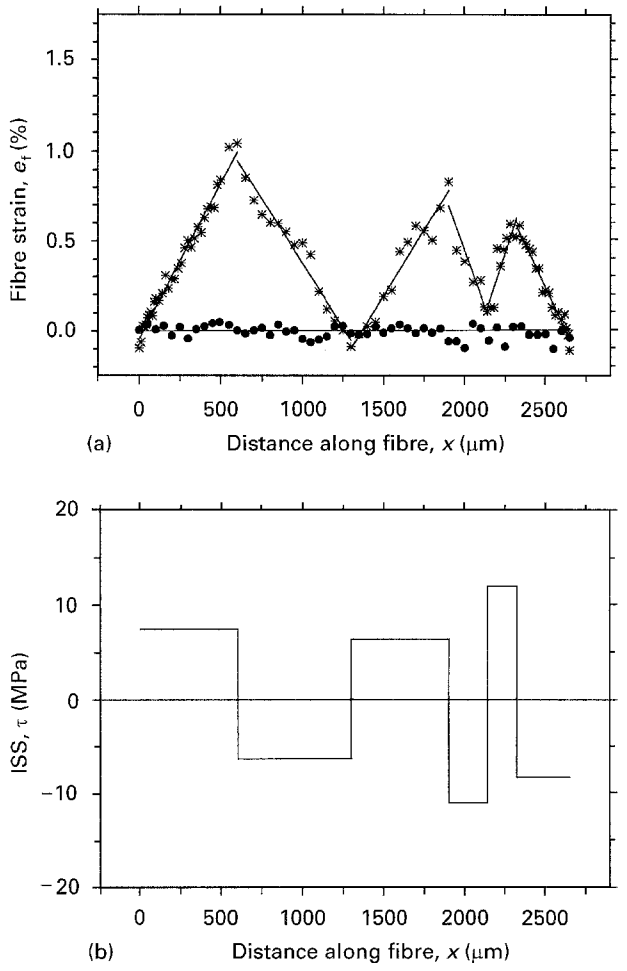

Figure 27 Variation of (a) fibre strain and (b) interfacial shear stress along the fragmented Kevlar 149 fibre shown in Figs 23b and 24b analysed using conventional fragmentation analysis. The matrix strains used were, (●) $e_m = 0\%$ and (*) $e_m = 2.0\%$.

The interfacial shear strength calculated from the fragmentation data was determined following fibre fracture which occurred for the Kevlar 149/epoxy system well after the maximum value of interfacial shear stress has been attained. The maximum value of interfacial shear stress occurred at the onset of matrix yielding at the fibre/matrix interface, i.e. when $e_m \sim 0.8\%$, after which point the value of τ_{max} decreases, as shown in Fig. 28. This indicates that the maximum interfacial shear stress is dependent only upon the shear yield stress of the resin. This is not apparent from the values of interfacial shear strength, τ_s, calculated from the saturated fragmentation data which are calculated only at high strain levels well after failure of the interface. This may also explain why Kalantar and Drzal did not observe any noticeable differences in the values of interfacial shear strength for aramid/epoxy model composites cured at different temperatures calculated using fragmentation tests [1]. More importantly it indicates that interfacial failure may take place prior to the onset of fibre fragmentation making the single-fibre fragmentation test unsuitable for the interfacial failure analysis of aramid fibres and possibly other fibre/matrix systems. In many cases the fragmentation test cannot be used for aramid fibres since the failure strain of the fibre may exceed that of the matrix.

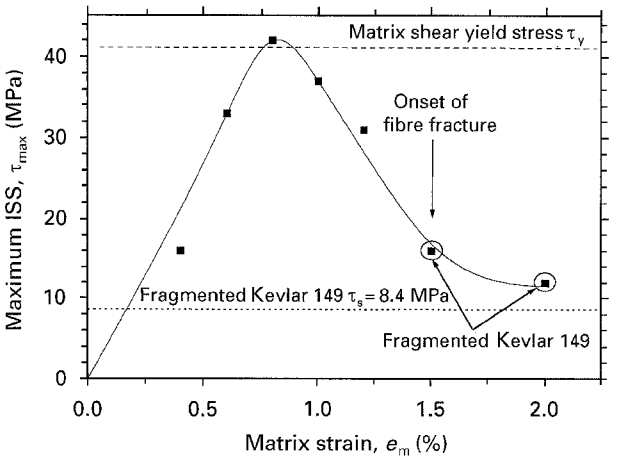

Figure 28 Dependence of maximum interfacial shear stress, τ_{max}, upon matrix strain for Kevlar 149 fibres in an epoxy resin matrix at different levels of strain.

4. Conclusions

It has been shown that the Raman technique can be used to monitor the variation of fibre strain along an aramid fibre inside an epoxy resin matrix from which the interfacial shear stress can be derived. It has also been demonstrated that the interfacial properties of aramid/epoxy model composites can be derived at different loading levels enabling the progressive failure of the fibre/matrix interface to be monitored.

At low strain levels it has been shown that the distribution of fibre strain and derived interfacial shear stress are in agreement with the behaviour predicted by shear-lag theory. It has also been found for different aramid fibre/epoxy resin matrix model composites that the maximum interfacial shear stress is highly dependent upon the shear yield stress of the epoxy resin matrix. This indicates that there is efficient stress transfer between the epoxy resin matrix and the aramid fibre and also implies that there is a good adhesive bond at the fibre/matrix interface.

The effect of fibre surface treatments upon the level of interfacial adhesion has only been identified at high strain levels once the shear yield stress of the epoxy resin matrix had been exceeded. In the case of the untreated aramid fibres the interfacial shear stress was found to decrease close to the fibre end due to debonding of the fibre matrix interface. This behaviour has been modelled successfully using a partially-elastic model. The surface treated fibres showed little or no evidence of interfacial debonding. However, for both the untreated and the surface treated aramid fibres the maximum interfacial shear stress was close to the shear yield stress of the epoxy resin matrix.

Raman spectroscopy has been found to be extremely powerful technique for monitoring the deformation of model composites using conventional micromechanical test methods. It has been clearly shown that the assumption of constant interfacial shear stress is inappropriate for determining the interfacial shear strength of a model composite. It has also been found that the maximum interfacial shear stress during

a pull-out test occurs well before the fibre pulls out from the resin matrix. It was also noticed that the values of interfacial shear strength calculated from a saturated fibre fragmentation test were considerably lower than the maximum value of interfacial shear stress calculated prior to fragmentation. Hence great care must be exercised in the determination of interfacial parameters using conventional micromechanical test methods. The findings of earlier workers that the values of interfacial shear strength are dependent upon the geometry of the micromechanical test method employed have been explained using the Raman analysis. It has also been found that the maximum values of interfacial shear stress, τ_{max}, derived at different loading levels, can be used to characterize the interfacial properties of aramid/epoxy model composites.

Acknowledgements

This work was supported by Research Grants from the Engineering and Physical Sciences Research Council, the Ministry of Defence and from Shell Research. One of the authors (R.J.Y.) is grateful to the Royal Society for support in the form of the Wolfson Research Professorship in Materials Science. The authors are also grateful to Dr R. J. Day (UMIST, Manchester), Dr J. Mahy (Akzo Nobel, Arnhem) and Dr A. J. Cervenka (Shell Research, Amsterdam) for the supply of data and helpful discussions during the course of this work.

References

1. J. KALANTAR and L. T. DRZAL, *J. Mater. Sci.* **25** (1990) 4194.
2. M. BREZNICK, J. BANBAJI, H. GUTTMANN and G. MAROM, *Polym. Comm.* **28** (1987) 55.
3. Y. WU and G. G. TESORO, *J. Appl. Polym. Sci.* **31** (1986) 1041.
4. L. S. PENN, T. J. BYERLEY and T. K. LIAO, *J. Adhesion* **23** (1987) 163.
5. M. R. WERTHEIMER and H. P. SCHREIBER, *J. Appl. Polym. Sci.* **26** (1981) 2087.
6. F. P. M. MERCX and P. J. LEMSTRA, *Polym. Comm.* **31** (1990) 252.
7. J. MAHY, L. W. JENNESKENS and O. GRABANDT, *Composites* **25** (1994) 653.
8. European Patent Specification No. 010787 (1987).
9. K. W. ALLEN, *J. Adhesion* **21** (1987) 261.
10. J. KALANTAR and L. T. DRZAL, *J. Mater. Sci.* **25** (1990) 4186.
11. F. PONCIN-EPAILLARD, B. CHEVET and J-C BROSSE, *J. Appl. Polym. Sci.* **52** (1994) 1047.
12. P. J. C. CHAPPELL and D. R. WILLIAMS, *J. Colloid Interface Sci.* **128** (1989) 450.
13. L. J. BROUTMANN, "Interfaces in Composites", ASTM STP 452, 1969, p. 27.
14. B. MILLER, P. MURI and L. REBENFELD, *Comp. Sci. and Tech.* **28** (1987) 17.
15. P. J. HERRERA-FRANCO and L. T. DRZAL, *Composites* **23** (1992) 2.
16. A. KELLY and W. R. TYSON, *J. Mech. Phys. Solids.* **13** (1965) 329.
17. J. F. MANDELL, D. H. GRANDE, T. H. TSIANG and F. J. McGARRY in Proceedings of 'Composite Materials Testing and Design' (Seventh Conference), ASTM STP 893, edited by J. M. Whitney (American Society for Testing and Materials, Philadelphia, 1986) p. 87.
18. M. J. PITKETHLY, J. P. FAVRE, U. GAUR, J. JAKUBOWSKI, S. F. MUDRICH, D. L. CALDWELL, L. T. DRZAL, M. NARDIN, H. D. WAGNER,L. DILANDRO, A. HAMPE, J. P. ARMISTEAD, M. DESAEGER and I. VERPOEST, *Comp. Sci. and Tech.* **48** (1993) 205.
19. A. HAMPE and C. MAROTZKE, Paper presented at workshop meeting, 'Interfaces in carbon, glass and polymer fibre reinforced composites', Kaiserslautern, February, 1995.
20. D. J. BANNISTER, M. C. ANDREWS, A. J. CERVENKA and R. J. YOUNG, *Comp. Sci. and Tech.* **53** (1995) 411.
21. H. D. WAGNER, H. E. GALLIS and E. WIESEL, *J. Mater. Sci.* **28** (1993) 2238.
22. A. N. NETRAVALI, Z-F LI, W. SACHSE and H. F. WU, *ibid.* **28** (1991) 6631.
23. K. PRASAD and D. R. GRUBB, *J. Polym. Sci.: Part B: Polym. Phys.* **27** (1989) 381.
24. B. J. KIP, M. C. P. VAN EIJK and R. J. MEIER, *ibid.* **29** (1991) 99.
25. R. J. DAY, I.M. ROBINSON, M. ZAKIKHANI and R. J. YOUNG, *Polymer* **28** (1987) 1833.
26. R. J. YOUNG, R. J. DAY and M. ZAKIKHANI, *Mat. Res. Soc. Symp. Proc.* **134** (1989) 351.
27. C. GALIOTIS, I. M. ROBINSON, R. J. YOUNG, B. J. E. SMITH and D. N. BATCHELDER, *Polym. Comm.* **26** (1985) 354.
28. S. VAN DER ZWAAG, M. G. NORTHOLT, R. J. YOUNG, C. GALIOTIS, I. M. ROBINSON and D. N. BATCHELDER, *ibid.* **28** (1987) 276.
29. Y. HUANG and R. J. YOUNG, *J. Mater. Sci. Lett.* **12** (1993) 92.
30. R. J. YOUNG, D. LU, R. J. DAY, W. F. KNOFF and H. A. DAVIS, *J. Mater. Sci.* **27** (1992) 5431.
31. X. YANG, X. HU, R. J. DAY and R. J. YOUNG, *ibid.* **27** (1992) 1409.
32. C. GALIOTIS, R. J. YOUNG, P. H. J. YEUNG and D. N. BATCHELDER, *ibid.* **19** (1984) 3640.
33. I. M. ROBINSON, R. J. YOUNG, C. GALIOTIS and D. N. BATCHELDER, *ibid.* **22** (1984) 3642.
34. H. JAHANKHANI and C. GALIOTIS, *J. Comp. Mater.* **25** (1991) 609.
35. C. GALIOTIS, *Comp. Sci. and Tech.* **42** (1991) 125.
36. M. C. ANDREWS and R. J. YOUNG, *J. Raman Spec.* **24** (1993) 539.
37. *Idem, Mater. Sci. Eng.* **A184** (1994) 197.
38. M. C. ANDREWS, R. J. YOUNG and J. MAHY, *Comp. Interfaces* **2** (1995) 433.
39. N. MELANITIS, C. GALIOTIS, P. L. TETLOW and C. K. L. DAVIES, *Composites* **24** (1993) 459.
40. R. J. YOUNG, Y-L HUANG, X. GU and R. J. DAY, *Plastics and Rubber Composites Processing and Applications* **23** (1995) 11.
41. L. C. N. BOOGH, R. J. MEIER, H. H. KAUSCH and B. J. KIP, *J. Polym. Sci.: Part B: Polym. Phys.* **30** (1992) 325.
42. Z-F LI and D. T. GRUBB, *J. Mater. Sci.* **29** (1994) 189.
43. D. T. GRUBB and Z-F LI, *ibid.* **29** (1994) 203.
44. R. J. YOUNG and P. I. GONZALES-CHI, *J. Mater. Sci. Lett.* **13** (1994) 1524.
45. X. YANG and R. J. YOUNG, *Composites* **25** (1994) 488.
46. M. C. ANDREWS, R. J. YOUNG and R. J. DAY, in "Developments in the Science and Technology of Composite Materials", edited by A. R. Bunsell, A. Kelly and A. Massiah (Woodhead Publishing Ltd., Cambridge, 1993) p. 133.
47. M. C. ANDREWS, A. K. PATRIKIS and R. J. YOUNG, Paper 32 presented at FRC'94 conference, Newcastle, March, 1994 (Institute of Materials, London, 1994).
48. N. MELANITIS and C. GALIOTIS, *Proc. R. Soc. Lond.* **A440** (1993) 379.
49. M. C. ANDREWS, R. J. DAY, A. K. PATRIKIS and R. J. YOUNG, *Composites* **25** (1994) 745.
50. A. K. PATRIKIS, M. C. ANDREWS and R. J. YOUNG, *Comp. Sci. and Tech.* **52** (1994) 387.
51. R. J. DAY and M. MARQUEZ, in "Interfacial Phenomena in Composite Materials, 91", edited by I. Verpoest and F. R. Jones (Butterworth-Heinemann, Oxford, 1991) p. 65.

52. M. C. ANDREWS and R. J. YOUNG, *J. Mater. Sci.* **30** (1995) 5607.
53. Q. MA, L. C. LIANG, D. R. CLARKE and J. W. HUTCHINSON, *Acta Metall. Mater.* **42** (1994) 3299.
54. R. J. YOUNG, D. LU and R. J. DAY, *Polym. Int.* **24** (1991) 71.
55. H. L. COX, *Br. J. Appl. Phys.* **3** (1952) 72.
56. M. R. PIGGOTT, "Load Bearing Fibre Composites" (Pergamon, Oxford, UK, 1980) p. 83.
57. T. H. LACROIX, B. TILMANS, R. KEUNINGS, M. DESAEGER and I. VERPOEST, *Comp. Sci. and Tech.* **43** (1992) 379.
58. T. H. LACROIX, R. KEUNINGS, M. DESAEGER and I. VERPOEST, *J. Mater. Sci.* **30** (1995) 683.
59. J. A. NAIRN, Y. C. LIU and C. GALIOTIS, ASTM STP (in press).
60. G. S. HOLISTER and C. THOMAS, "Fibre Reinforced Materials" (Elsevier Publishing Co. Ltd., London, 1966).
61. M. E. CATES and S. F. EDWARDS, *Proc. R. Soc. Lond.* **A395** (1984) 89.
62. C. F. FAN and S. L. HSU, *Macromolecules* **22** (1989) 1474.
63. R. J. YOUNG, "Introduction to Polymers" (Chapman and Hall, London, 1981) p. 266.
64. D. R. ASKELAND, "The Science and Engineering of Materials", 2nd Edn. (Chapman and Hall, London, 1990).
65. C. VLATTAS and C. GALIOTIS, *Polymer* **32** (1991) 1788.
66. *Idem, ibid.* **35** (1994) 2335.
67. H. JAHANKHANI and C. GALIOTIS, in "Interfaces in Polymer, Ceramic and Metal Matrix Composites", edited by H. Ishida (Elsevier Science, New York, 1988) p. 107.
68. P. J. C. CHAPPELL, D. R. WILLIAMS and G. A. GEORGE, *J. Coll. and Int. Sci.* **134** (1990) 385.
69. Y-L HUANG and R. J. YOUNG, *Composites* **26** (1995) 541.
70. P. S. CHUA and M. R. PIGGOTT, *Comp. Sci. and Tech.* **22** (1985) 33.
71. R. J. DAY paper presented at Second International Conference on 'Deformation and Fracture of Composites', UMIST, Manchester, March 1993 (Institute of Materials, London, 1993) p. 23.
72. C. H. REINSCH, *Numer. Math.* **10** (1967) 177.

Received 24 May
and accepted 7 December 1995